Gas-phase chemistry in the online multiscale NMMB/BSC Chemical Transport Model: Description and evaluation at global scale

Alba Badia[1,*], Oriol Jorba[1], Apostolos Voulgarakis[2], Donald Dabdub[3], Carlos Pérez García-Pando[4, 5], Andreas Hilboll[6,7], María Gonçalves[1, 8], and Zavisa Janjic[9]

[1]Earth Sciences Department, Barcelona Supercomputing Center-Centro Nacional de Supercomputación, Barcelona, Spain
[2]Department of Physics, Imperial College, London
[3]Mechanical and Aerospace Engineering, University of California, Irvine
[4]NASA Goddard Institute for Space Studies, New York, USA
[5]Department of Applied Physics and Applied Math, Columbia University, New York, USA
[6]Institute of Environmental Physics, University of Bremen, Germany
[7]MARUM – Center for Marine Environmental Sciences, University of Bremen, Germany
[8]Universitat Politecnica de Catalunya, Barcelona, Spain
[9]National Centers for Environmental Prediction, College Park, MD, USA
[*]Now in the Centre for Ocean and Atmospheric Sciences, School of Environmental Sciences, University of East Anglia, Norwich, United Kingdom

Correspondence to: oriol.jorba@bsc.es

Abstract.

This paper presents a comprehensive description and benchmark evaluation of the tropospheric gas-phase chemistry component of the NMMB/BSC Chemical Transport Model (NMMB/BSC-CTM), an online chemical weather prediction system conceived for both the regional and the global scale. We provide an extensive evaluation of a global annual cycle simulation us-

5 ing a variety of background surface stations (EMEP, WDCGG and CASTNET), ozonesondes (WOUDC, CMD and SHADOZ), aircraft data (MOZAIC and several campaigns), and satellite observations (SCIAMACHY and MOPITT). We also include an extensive discussion of our results in comparison to other state-of-the-art models.

The model shows a realistic oxidative capacity across the globe. The seasonal cycle for CO is fairly well represented at different locations (correlations around 0.3-0.7 in surface concentrations), although concentrations are underestimated in spring and

10 winter in the Northern Hemisphere, and are overestimated throughout the year at 800 and 500 hPa in the Southern Hemisphere.

Nitrogen species are well represented in almost all locations, particularly NO_2 in Europe (RMSE below 9 μg m^{-3}). The modeled vertical distribution of NO_x and HNO_3 are in excellent agreement with the observed values and the spatial and seasonal trends of tropospheric NO_2 columns correspond well to observations from SCIAMACHY, capturing the highly polluted areas and the biomass burning cycle throughout the year. Over Asia, the model underestimates NO_x from March to August

15 probably due to an underestimation of NO_x emissions in the region. Overall, the comparison of the modelled CO and NO_2 with MOPITT and SCIAMACHY observations emphasizes the need for more accurate emission rates from anthropogenic and biomass burning sources (i.e., specification of temporal variability).

The resulting ozone (O_3) burden (348 Tg) lies within the range of other state-of-the-art global atmospheric chemistry models. The model generally captures the spatial and seasonal trends of background surface O_3 and its vertical distribution. However,

Geoscientific
Model Development
Discussions

the model tends to overestimate O_3 throughout the troposphere in several stations. This is attributed to an overestimation of CO concentration over the southern hemisphere leading to an excessive production of O_3. Overall, O_3 correlations range between 0.6 to 0.8 for daily mean values. The overall performance of the NMMB/BSC-CTM is comparable to that of other state-of-the-art global chemical transport models.

1 Introduction

Tropospheric ozone (O_3) is a radiatively active gas interacting with solar and terrestrial radiation that is mainly produced during the photochemical oxidation of methane (CH_4), carbon monoxide (CO) and non-methane volatile organic compounds (NMVOC) in the presence of nitrogen oxides (NO_x) (Crutzen, 1974; Derwent et al., 1996). Downward transport from the stratosphere, where O_3 is created by photolysis of oxygen (O_2) molecules, is also an important source of tropospheric O_3 (Stohl et al., 2003; Hsu and Prather, 2009). In urban areas, O_3 is a major component of 'smog', which can cause a number of respiratory health effects (WHO, 2014). Since the pre-industrial era, changes in emissions of O_3 precursors from anthropogenic and biomass burning sources have modified the distribution of tropospheric O_3 and other trace gases (Lamarque et al., 2013). Tropospheric O_3, with an average lifetime of the order of weeks, is highly variable in space and time, and Air Quality Models (AQM) are required to predict harmful levels of O_3 along with its precursors and other trace gases.

AQMs are driven by meteorological fields and fed by emission inventories. They include a chemical mechanism for representing gas-phase and aerosol atmospheric chemistry, a photolysis scheme describing the photo-dissociation reactions driven by sunlight, dry and wet deposition schemes to account for the removal of pollutants from the atmosphere, and the characterization of the downward transport of stratospheric O_3. The development of AQMs and meteorological models (MM) evolved as separate fields (offline approach) due to complexity and limitations in computer resources.

The offline approach requires lower computational capacity, but involves a loss of essential information on atmospheric processes whose time-scale is smaller than the output time rate of the meteorological model (Baklanov et al., 2014). Nowadays, owing to a general increase in computer capacity, online coupled meteorology-chemistry models are being increasingly developed and used by the scientific community, who recognizes the advantages of the online approach (Byun, 1990). Overviews of online AQM-MM models are available in the literature (Zhang, 2008; Baklanov et al., 2014).

Several global AQMs have been developed during the last decades: online multiscale GEM-AQ (1.5° x 1.5°) (Gong et al., 2012), offline TM5-chem-v3.0 (3° x 2°) (Huijnen et al., 2010), online LMDZ-INCA (3.8° x 2.5°) (Folberth et al., 2006), online GATOR-GCMM (4° x 5°) (Jacobson, 2001), online IFS-MOZART used in MACC project (80km x 80km) (Inness et al., 2013), online C-IFS recently developed at ECMWF (80km x 80km) (Flemming et al., 2015), and offline MOZART-4 (2.8° x 2.8°) (Emmons et al., 2010). Most of these models have been applied at coarse resolutions with simplified chemical schemes. Currently, the systems are being updated and prepared for higher resolution applications.

In this contribution, we describe and evaluate the gas-phase chemistry of the NMMB/BSC Chemical Transport Model (NMMB/BSC-CTM), an online multi-scale non-hydrostatic chemical weather prediction system that can be run either globally

Geoscientific
Model Development
Discussions

or regionally (Pérez et al., 2011; Jorba et al., 2012). We provide a thorough evaluation over a one-year period for the global domain using an horizontal resolution of $1° \times 1.4°$.

The NMMB/BSC-CTM model, configured as a limited area model, has recently participated in the Air Quality Model Evaluation International Initiative Phase2 (AQMEII-Phase2) intercomparison exercise. A spatial, temporal and vertical evaluation

5   of the chemical model results for the year 2010 on a regional scale are presented in Badia and Jorba (2014). Moreover, a comparison between other modeling systems currently applied in Europe and North America in the context of AQMEII phase 2 is presented in Im et al. (2014). Evaluations of previous version of the model include the dust implementation, presented in Pérez et al. (2011) and Haustein et al. (2012), and the sea-salt aerosol module, described and evaluated at the global scale in Spada et al. (2013) and Spada et al. (2015). The aerosol module for other relevant global aerosols (natural, anthropogenic and sec-

10   ondary) is currently under development within the NMMB/BSC-CTM (Spada et al., in prep). This initiative aims at developing a fully coupled chemical multiscale (global/regional) weather prediction system that resolves gas-aerosol-meteorology interactions and provides initial and boundary conditions for embedded high resolution nests in a unified dynamics-physics-chemistry environment.

The focus of this paper is to describe and evaluate the global atmospheric model NMMB/BSC-CTM in terms of the spatial

15   distribution and seasonal variations of O_3 and its precursors. In Sec. 2, we provide a description of the atmospheric driver, the gas-phase chemistry module, and the model configuration including the online biogenic emissions. Section 3 presents an overview of the model setup with a description of the chemical and meteorological initial conditions, and the anthropogenic and biomass burning emissions implemented for this experiment. We illustrate the capability of the NMMB/BSC-CTM to reproduce the main reactions occurring in the atmosphere by evaluating the model with ground-based monitoring stations,

20   ozonesondes, aircraft data, climatological vertical profiles and satellite retrievals, which are described in Sec. 4. The results of the model performance are discussed in Sec. 5 for year 2004. The last section summarizes the conclusions of this work.

2   Model description

The NMMB/BSC-CTM is a fully online multiscale chemical transport model for regional and global-scale applications (Pérez et al., 2011; Jorba et al., 2012). The system is based on the meteorological Non-hydrostatic Multiscale Model on B-grid

25   (NMMB; Janjic and Gall, 2012), developed at the National Centers for Environmental Prediction (NCEP). The model couples online the NMMB with the gas-phase and aerosol continuity equations to solve the atmospheric chemistry processes with detail. Due to its online-coupling approach, the model accounts for the feedback processes of gases, aerosol particles and radiation. Currently, it can consider the radiative effect of aerosols while presently ignoring cloud-aerosol interactions. In the present work, only the gas-phase chemistry is used, thus no interaction between gas-phase and aerosol-phase is applied. In this

30   section we provide a concise description of the NMMB model and the gas-phase chemistry module of the BSC-CTM.

2.1 The Non-hydrostatic Multiscale Model on B-grid

The Non-hydrostatic Multiscale Model on B grid(NMMB; Janjic and Black, 2005; Janjic and Gall, 2012) was conceived for short- and medium-range forecasting over a wide range of spatial and temporal scales from large eddy simulations (LES) to global simulations. Its unified non-hydrostatic dynamical core allows regional and global simulations, including embedded

5   regional nests. The NMMB has been developed within the Earth System Modeling Framework (ESMF) at NCEP, following the general modeling philosophy of the NCEP regional Weather Research and Forecasting (WRF) Non-hydrostatic Mesoscale Model (NMM; Janjic et al., 2001; Janjic, 2003). The regional NMMB has been the operational regional North American Mesoscale (NAM) model at NCEP since October 2011. The numerical schemes used in the model were designed following the principles presented in Janjic (1977, 1979, 1984, 2003). Isotropic horizontal finite volume differencing is employed so a variety

10 of basic and derived dynamical and quadratic quantities are conserved. Among these, the conservation of energy and entrophy (Arakawa, 1966) improves the accuracy of the nonlinear dynamics. The hybrid pressure-sigma coordinate is used in the vertical direction and the Arakawa B-grid is applied in the horizontal direction. The global model on the latitude-longitude grid with polar filtering was developed as the reference version, and other geometries such the cubed-sphere are currently being tested. The regional model is formulated on a rotated longitude-latitude grid, with the Equator of the rotated system running through

15 the middle of the integration domain resulting in more uniform grid distances. The non-hydrostatic component of the model dynamics is introduced through an add-on module that can be turned on or off, depending on the resolution. The operational physical package includes: (1) the Mellor-Yamada-Janjic (MYJ) level 2.5 turbulence closure for the treatment of turbulence in the planetary boundary layer (PBL) and in the free atmosphere (Janjic et al., 2001), (2) the surface layer scheme based on the Monin-Obukhov similarity theory (Monin and Obukhov, 1954) with introduced viscous sublayer over land and water

20 (Zilitinkevich, 1965; Janjic, 1994), (3) the NCEP NOAH (Ek et al., 2003) or the LISS land surface model (Vukovic and Z., 2010) for the computation of the heat and moisture surface fluxes, (4) the GFDL or RRTMG long-wave and shortwave radiation package (Fels and Schwarzkopf, 1975; Mlawer et al., 1997), (5) the Ferrier gridscale clouds and microphysics (Ferrier et al., 2002), and (6) the Betts-Miller-Janjic convective parametrization (Betts, 1986; Betts and Miller, 1986; Janjic, 1994, 2000). Vertical diffusion is handled by the surface layer scheme and by the PBL scheme. Lateral diffusion is formulated following the

25 Smagorinsky non-linear approach (Janjic, 1990).

2.2 Gas-phase chemistry module

The tropospheric gas-phase chemistry module is coupled online within the NMMB code. Different chemical processes were implemented following a modular operator splitting approach to solve the advection, diffusion, chemistry, dry and wet deposition, and emission processes. Meteorological information is available at each time step to solve the chemical processes

30 properly. In order to maintain consistency with the meteorological solver, the chemical species are advected and mixed at the corresponding time step of the meteorological tracers using the same numerical schemes implemented in the NMMB. The advection scheme is Eulerian, positive definite and monotone, maintaining a consistent mass-conservation of the chemical species within the domain of study (Janjic et al., 2009; Tang et al., 2009; Janjic and Gall, 2012).

2.2.1   Chemical-phase reaction mechanism

Several chemical mechanisms can be implemented within the NMMB/BSC-CTM. A modular coupling with the Kinetic Pre-Processor (KPP) package (Damian et al., 2002; Sandu and Sander, 2006) allows the model to maintain wide flexibility. Additionally, an Eulerian-Backward-Iterative solver (Hertel et al., 1993) was implemented as a complementary option to the KPP

5   solvers to allow the model to run with a fast ordinary differential equation solver at global scales. For the present study, we use a Carbon-Bond family mechanism, the Carbon Bond 2005 (CB05; Yarwood et al., 2005), an updated version of the Carbon-Bond IV (CB4) lumped-structure-type mechanism (Gery et al., 1989). CB4 was formulated focusing on limited domain extent, urban and regional environments and for planetary boundary layer chemistry. CB05 extends its applicability from urban to remote tropospheric conditions and is suitable for global applications. CB05 was evaluated against smog chamber data from the

10   University of California, Riverside and University of North Carolina. It includes 51 chemical species and solves 156 reactions (see Tables S1 and S2 in the supplementary information). Both the organic chemistry of methane and ethane, and the chemistry of methylperoxy radical, methyl hydroperoxide and formic acid are treated explicitly. The higher organic peroxides, organic acids, and peracids are treated as lumped species. Following its main design, CB05 defines proxy single and double carbon bond species, paraffin and an olefin bond respectively, and it introduces the internal olefin species. The rate constants were

15   updated based on evaluations from Atkinson et al. (2004) and Sander et al. (2006). Organic compounds not explicitly treated are apportioned to the carbon-bond species based on the molecular structure and following Yarwood et al. (2005) assignments from VOC species to CB05 model species. The concentration of methane is considered constant (1.85 ppm) in this study.

2.2.2   Photolysis scheme

One of the most important processes determining tropospheric composition is the photo-dissociation of trace gases. Table S2

20   in the supplementary information lists the photolysis reactions considered. To compute the photolysis rates, we implemented the Fast-J (Wild et al., 2000) online photolysis scheme. Fast-J has been coupled with the physics of each model layer (e.g., clouds and absorbers such as O_3). The optical depths of grid-scale clouds from the atmospheric driver are considered by using the fractional cloudiness based on relative humidity (Fast et al., 2006). The main advantages of Fast-J are the optimization of the phase function expansion into Legendre polynomials and the optimization of the integration over wavelength (Wild et al.,

25   2000). The Fast-J scheme has been upgraded with CB05 photolytic reactions. The quantum yields and cross section for the CB05 photolysis reactions have been revised and updated following the recommendations of Atkinson et al. (2004) and Sander et al. (2006). The Fast-J scheme uses seven different wavelength bins appropriate for the troposphere to calculate the actinic flux covering from 289 to 850 nm (see Table VIII from Wild et al. (2000)). In this work, aerosols are not considered in the photolysis rate calculation.

30   ### 2.2.3   Dry-deposition scheme

The dry-deposition scheme is responsible for computing the flux of trace gases from the atmosphere to the surface. It is calculated by multiplying concentrations in the lowest model layer by the spatially and temporally varying deposition velocity:

Geoscientific
Model Development
Discussions

$$\frac{\partial C_i}{\partial t}\bigg|_{dry-dep} = -C_i v_d \tag{1}$$

where t is the time, i the gas-phase species, C_i is the concentration of the gas in the lowest model layer, and v_d is the dry-deposition velocity. At each time step, v_d is calculated according to:

$$|v_d| = \frac{1}{(R_a + R_b + R_c)} \tag{2}$$

where R_a is the aerodynamic resistance (depends only on atmospheric conditions), R_b is the quasilaminar sublayer resistance (depends on friction velocity and molecular characteristics of gases), and R_c is the canopy or surface resistance (depends on surface properties and the reactivity of the gas). R_a and R_b are computed following their common definition (Seinfeld and Pandis, 1998), while R_c is simulated following Wesely (1989), where the surface resistance is derived from the resistances of the surfaces of the soil and the plants. The properties of the plants are determined using land-use data (from the meteorological driver USGS land-use) and depend on the season. The surface resistance also depends on the diffusion coefficient, the reactivity, and water solubility of the reactive trace gases.

2.2.4 Wet-deposition scheme

We use the scheme of Byun and Ching (1999) and Foley et al. (2010) to resolve the cloud processes affecting the concentration of 36 gases from the CB05 chemical mechanism. The processes included are grid-scale scavenging and wet-deposition, subgrid-scale vertical mixing, and scavenging and wet-deposition for precipitating and non-precipitating clouds. At the moment, we consider only in-cloud scavenging, which is computed using the Henry's Law equilibrium equation. The rate of change for in-cloud pollutant concentration is given by:

$$\frac{\partial C_{icld}}{\partial t} = C_{icld} \frac{e^{-\alpha_i \tau_{cld}} - 1}{\tau_{cld}} \tag{3}$$

where C_{icld} is the gas concentration within the cloud [ppm], τ_{cld} is the cloud timescale [s], and α_i is the scavenging coefficient for the gas species that is calculated as:

$$\alpha_i = \frac{1}{\tau_{washout}(1 + \frac{TWF}{H_i})}, \tag{4}$$

where H_i is the Henry's Law coefficient for the gas species [M/atm], TWF=$\rho_{H_2O}/(W_T RT)$ is the total water fraction (where W_T is the total mean water content [M/atm], R is the Universal gas constant, and T is the in-cloud air temperature [K]), and $\tau_{washout}$ is the washout time [s], i.e., the amount of time required to remove all of the water from the cloud volume at a specified precipitation rate [m/s], which is given by:

$$\tau_{washout} = \frac{W_T \Delta Z_{cld}}{\rho_{H_2O} P_r} \tag{5}$$

where ΔZ_{cld} is the cloud thickness [m] and P_r is the precipitation rate [m/s]. Both grid-scale and subgrid-scale scavenging are computed with equation 3, where τ_{cld} is 1 hour for subgrid-scale clouds, and the chemistry timestep for grid-scale clouds. Wet deposition is computed following the algorithm of Chang et al. (1987), which depends upon P_r and the gas concentration within the cloud C_{icld}. Thus, the wet deposition is given by:

$$wdep_i = \int_0^{\tau_{cld}} C_{icld} P_r dt \tag{6}$$

The sub-grid cloud scheme implemented solves convective mixing, scavenging and wet deposition of a representative cloud within the grid cell following the CMAQ and RADMv2.6 model schemes (Byun and Ching, 1999; Chang et al., 1987). Precipitating and non-precipitating sub-grid clouds are considered. The latter are categorized as pure fair weather clouds and non-precipitating clouds and may coexist with precipitating clouds (Byun and Ching, 1999; Foley et al., 2010).

2.2.5 Upper boundary conditions

Because the model focuses on the troposphere, stratospheric chemistry is taken into account using a simplified approach. Above 100 hPa, mixing ratios of several species (NO, NO_2, N_2O_5, HNO_3 and CO) are initialized each day from a global chemical model MOZART-4 (Emmons et al., 2010). For O_3, an important reactive gas requiring a more refined representation in the stratosphere, we use a linear O_3 stratospheric scheme, COPCAT (Monge-Sanz et al., 2011). COPCAT is based on the approach of Cariolle and Déqué (1986), which represented the first effort to include a linearized O_3 scheme (named Cariolle v1.0) in a three-dimensional model.

Following the COPCAT approach, the change in O_3 with time due to local chemistry is given by:

$$\frac{\partial C_{O_3}}{\partial t} = \frac{d\chi}{dt} = (P-L)[\chi, T, \Phi] \tag{7}$$

where $(P-L)$ represents the O_3 tendency as a linear function depending on χ, the O_3 mass mixing ratio ($kg\,kg^{-1}$), T, the temperature (K), and Φ, the column O_3 above the point under consideration ($kg\,m^{-2}$).

Equation (7) is expanded to first order in a Taylor Series as follows:

$$\frac{\partial C_{O_3}}{\partial t} = \frac{d\chi}{dt} = (P-L)_0 + \overbrace{\left.\frac{\partial(P-L)}{\partial \chi}\right|_0 (\chi - \chi_0)}^{\mathbf{a}} +$$
$$\overbrace{\left.\frac{\partial(P-L)}{\partial T}\right|_0 (T - T_0)}^{\mathbf{b}} + \overbrace{\left.\frac{\partial(P-L)}{\partial \Phi}\right|_0 (\Phi - \Phi_0)}^{\mathbf{c}} \tag{8}$$

The second term in the expansion represents variations in the local O_3 amount (a), the third represents temperature effects (b) and the last term, called radiation term, accounts for the influence of non-local O_3 on the amount of solar radiation reaching the level under consideration (c). Specific terms in this equation (represented with the subscript 0) are coefficients applicable at the equilibrium state. In COPCAT these coefficients are obtained at equilibrium from the TOMCAT/SLIMCAT box model (Chipperfield, 2006). These terms are presented as functions of 24 latitudes, 24 model vertical levels and 12 months.

Heterogeneous processes describing the polar stratospheric chemistry are non-linear and depend on the three-dimensional structure of the atmosphere. COPCAT includes complete heterogeneous processes in their coefficients, considering heterogeneous and gas-phase chemistry to be consistent when applied in this linear O_3 parameterization. This kind of parameterization is in better agreement with the current state of knowledge of stratospheric heterogeneous chemistry than previous schemes (Monge-Sanz et al., 2011). For further description of the approach, the reader is referred to Monge-Sanz et al. (2011).

2.2.6 Online natural emissions

Natural emissions of gaseous pollutants include biogenic emissions, soil emissions, emissions from lightning, and emissions from oceans and volcanoes. Currently, soil and oceanic emissions in the model are prescribed as described in Sect. 3.1 and emission from lightning and volcanoes are not considered. Only biogenic emissions, which strongly depend on meteorological fields and vegetation cover, are calculated online. They are computed using the Model of Emissions of Gases and Aerosols from Nature version 2.04 (MEGANv2; Guenther et al., 2006). MEGAN is able to estimate the net emission rate of gases and aerosols from terrestrial ecosystems into the above-canopy atmosphere. MEGAN canopy-scale emission factors differ from most other biogenic emission models, which use leaf-scale emission factors, and cover more than 130 Non-Methane Volatile Organic Compounds (NMVOCs). All the MEGAN NMVOCs are speciated following the CB05 chemical mechanism; thus, emissions for isoprene, lumped terpenes, methanol, nitrogen monoxide, acetaldehyde, ethanol, formaldehyde, higher aldehydes, toluene, carbon monoxide, ethane, ethene, paraffin carbon bond, and olefin carbon bond are considered within the model. Biogenic emissions are computed every hour to account for evolving meteorological changes in solar radiation and surface temperature. Thus, weather- driving variables considered are temperature at 2 m and incoming short wave radiation at surface.

Figure S1 in the supplementary information shows the modeled emission for isoprene and terpenes for January and July 2004, and Table 2 lists the global annual emissions for isoprene, monoterpenes and other important NMVOCs. Biogenic isoprene emissions used in this study amount 683.16 Tg/year. While other global models have lower estimates (Huijnen et al., 2010; Horowitz et al., 2003; Emmons et al., 2010), MEGAN isoprene emissions typically range from about 500 to 750 Tg/year (Guenther et al., 2006). These estimates largely depend on the assumed land cover, emission factors, and meteorological parameters Therefore, the emission uncertainties and their impacts upon surface O_3 are associated with uncertainties in these inputs. Ashworth et al. (2010) obtained emission reductions of 3% and 7% when using daily and monthly meteorological data, respectively, instead of hourly data, with reductions reaching up to 55% in some locations. Marais et al. (2014) performed several sensitivity model runs to study the impact of different model input and settings on isoprene estimates that resulted in differences of up to $\pm$ 17% compared to a baseline. In our study, weather inputs are based on previous day 24h averages and data of the hour of interest.

3   Model setup

The model is set up as global with a horizontal grid spacing of $1.4° x 1°$ and 64 vertical layers up to 1 hPa. The dynamics fundamental time step is set to 180s and the chemistry processes are solved every 4 fundamental time steps. The radiation, photolysis scheme and biogenic emissions are computed every hour. We use NCEP/Final Analyzes (FNL) as initial conditions

5   for the meteorological driver, and we reinitialize the meteorology every 24 h to reproduce the observed transport. We performed a spin-up of 1-year using initial chemistry conditions from the global atmospheric model MOZART-4 Emmons et al. (2010) prior to the 2004 annual cycle simulation that is evaluated in the present study. Table 1 describes the main configuration of the model. The feedback between chemistry and meteorology is not considered in this study.

3.1   Emissions

10   The global emissions used in this study are based on the Atmospheric Chemistry and Climate Model Intercomparison Project (ACCMIP; Lamarque et al., 2013), which includes emissions from anthropogenic and biomass burning sources at $0.5° x0.5°$ horizontal resolution (Lamarque et al., 2010). Note that the 2004 emissions are derived from a linear interpolation between years 2000 and 2010. Therefore specific events occurred during 2004 (e.g., large summer wildfires in Alaska and Canada) are not described. The ACCMIP inventory is a combination of several existing regional and global inventories. The surface

15   anthropogenic emissions are based on two historical emission inventories, namely RETRO (1960-2000; Schultz and Rast (2007)) and EDGAR-HYDE (1890-1990; Van Aardenne et al. (2005)) and monthly variations for biomass burning, ship and aircraft emissions are provided. One limitation is that land-based anthropogenic emissions have constant values for the entire year. Lamarque et al. (2010) presents a comparison of the annual total CO anthropogenic and biomass burning emissions (Tg(CO)/year) for different regional and global emission inventories for year 2000 (see Table 5 of this paper). Note that

20   ACCMIP global CO anthropogenic emissions are significantly higher (610.5 Tg CO/year) than other emissions inventories (e.g. RETRO with 476 Tg CO/year, EDGAR-HYDE with 548 Tg CO/year, and GAINS with 542 Tg CO/year).

Ocean and soil natural emissions are based on the POET (Granier et al., 2005) global inventory. Lightning and volcano emissions are not considered in this simulation. Biogenic emissions are computed using MEGANv2 model as described in Sec. 2.2.6. NO emissions for January and July 2004 are shown in Figure S1 in the supplementary information and yearly totals

25   for anthropogenic and biomass burning are summarized in Table 2.

To account for the sub-grid scale vertical diffusion within the planetary boundary layer (PBL) all the land-based anthropogenic emissions are emitted in the first 500 m of the model, biomass burning emissions from forests in the first 1300 m, biomass burning emissions from grass in the first 200 m, ocean emissions on the first 30 m and shipping emissions on the first 500 m. The model does not include the attenuation of radiation due to aerosols in the photolysis scheme. Therefore, regions

30   with strong biomass burning emissions may significantly overestimate chemical photolysis production.

4 Observational data

4.1 Surface concentration and wet deposition

For the evaluation of ground-level gas concentrations, we selected background stations having hourly data (Fig. 1) from the World Data Center for Greenhouse Gases (WDCGG; http://gaw.kishou.go.jp/wdcgg/), the European Monitoring and Evaluation Programme (EMEP; http://www.emep.int/), the Clean Air Status and Trends Network in USA (CASTNET; http://java.epa.gov/castnet/) and the Acid Deposition Monitoring Network in East Asia (EANET; http://www.eanet.asia/). For O_3, we used data from 41 WDCGG, 52 EMEP, 64 CASTNET and 11 EANET stations, covering Europe, United States, and a few locations in east Asia. We also selected 21 EMEP stations for NO_2, 10 EANET stations for NO_x and 14 WDCGG stations for CO.

The simulated wet deposition of HNO_3 is also compared against observed nitrate (HNO_3 and aerosol nitrate) wet deposition, including 260 measurements from the National Atmospheric Deposition Program (NADP; http://nadp.sws.uiuc.edu/) network in North America, 51 from the EMEP network in Europe and 28 from EANET in East Asia.

4.2 Vertical structure: ozonesondes and MOZAIC

The surface evaluation is complemented with an assessment of the vertical structure of O_3 using ozonosondes from the World Ozone and Ultraviolet Radiation Data Center ozonosonde network (WOUDC;http://www.woudc.org/), the Global Monitoring Division (GMD; ftp://ftp.cmdl.noaa.gov/ozwv/ozone/) and the Southern Hemisphere ADditional OZonesondes (SHADOZ; http://croc.gsfc.nasa.gov/shadoz/; Thompson et al., 2003a, b). Most stations provide between 4 and 12 profiles per month each year with a precision of ± 3-8 % in the troposphere (Tilmes et al., 2012). We followed the methodology of Tilmes et al. (2012) for the selection and treatment of the measurements. Table 3 lists the locations and the number of available measurements per season of the 39 ozonesonde stations used (also displayed in Fig. 1), as well as the regions where stations with similar O_3 profiles were aggregated).

Additional observations considered in this study are CO vertical profiles from Measurement of Ozone, Water Vapor, Carbon Monoxide, Nitrogen Oxide by Airbus In-Service Aircraft (MOZAIC; http://http://www.iagos.fr). Based on the availability of data, we selected 14 airports (displayed in Fig. 1) covering different regions of the world during 2004. The number of vertical profiles available per season are provided in Table 4.

Nitric oxide (NO_x), peroxyacetyl nitrate (PAN) and acid nitric (HNO_3) vertical profiles are used from two different measurement campaigns: TOPSE (Atlas et al., 2003; Emmons et al., 2003) and TRACE-P (Jacob et al., 2003). Tropospheric data from these two previous campaigns were gridded onto global maps with resolution 5°x5° x1km, forming data composites of important chemical species in order to provide a picture of the global distributions (Emmons et al., 2000).

When running an AQM model, it is preferable to compare the model output with an observational database from the same year as the model simulation. Nevertheless, in our case, there are insufficient global observations to achieve this goal for any full year. Hence, in this model evaluation, all the observations are for 2004, except for the vertical profiles obtained from measurement campaigns. Hence, in this study, model output from selected regions are compared with this campaign from the same regions regardless of the year of the measurements. In addition, it is valuable to compare the same regions for different

species which allows identification of systematic differences between the model results and observations (Emmons et al., 2000). Details of these campaigns describing their geographical region and period are described in Table 5, and the location displayed in Fig. 1 (right panel).

4.3 Satellite data

Modelled tropospheric NO_2 columns are compared with SCanning Imaging Absorption spectroMeter for Atmospheric CHartographY (SCIAMACHY, http://www.sciamachy.org/) satellite data. SCIAMACHY (on board of ENVISAT, which was operational from March 2002 to April 2012) is a passive remote sensing spectrometer measuring backscattered, reflected, transmitted or emitted radiation from the atmosphere and Earth's surface with a wavelength range between 240-2380 nm. The SCIAMACHY instrument has a spatial resolution of typically 60 x 30 km^2, and has three different viewing geometries: nadir, limb, and sun/moon occultation. Alternating nadir and limb views, global coverage is achieved in six days.

NO_2 daily data was obtained from the Institute of Environmental Physics, the University of Bremen (http://www.iup.uni-bremen.de/doas/scia_no2_data_tropos.htm), based on Version 3.0 data product (Hilboll et al., 2013). This dataset is an improved extension of the data presented in Richter et al. (2005). Validation of the data product was performed in several studies (e.g., (Petritoli et al., 2004), (Heue et al., 2005)). We used daily satellite overpasses of cloud-free (<20% cloud fraction) tropospheric vertical column densities (VCDtrop NO_2) from SCIAMACHY measurements using the limb/nadir matching approach, whose total uncertainty is estimated to vary between 35 and 60% in heavily polluted cases and >100% in clean scenarios (Boersma et al. (2004)).

Additionally, CO mixing ratios at 800 and 500 hPa were evaluated with the Measurement of Pollution in the Troposphere (MOPITT: http://www2.acd.ucar.edu/mopitt) instrument retrievals. The MOPITT, aboard the NASA EOS-Terra satellite, is a gas filter radiometer and measures thermal infrared (near 4.7 μm) and near-infrared (near 2.3 μm) radiation, only during clear-sky conditions, with a ground footprint of about 22 km x 22 km. We used the MOPITT Version 5 (V5) Level 2 data product, which provides daily CO mixing ratios. MOPITT CO mixing ratios have been validated with in situ CO profiles measured from numerous NOAA/ESRL aircraft profiles in Deeter et al. (2013), and they were found to be positively biased by about 1% and highly correlated (r = 0.98) at the surface level.

5 Model evaluation

This section presents the evaluation of relevant trace gases from the NMMB/BSC-CTM using the observations described in the previous section. It also compares the results with other modeling studies available in the literature. For the surface-level comparison, three-hourly averages from the observations and model are used to compute daily O_3 averages and calculate the statistical measures defined in section 1 in the supplemental material. Ground-monitoring stations were selected with a maximum altitude of 1000 meters. In the case of ozonesondes and MOZAIC the comparison is made only when vertical profile observations are available, i.e., the data from the model and the observations are collocated/simultaneous. Similar criteria is used in the case of MOPITT and SCIAMACHY for NO_2. Moreover, averaging kernels for CO are accounted to represent

Geoscientific
Model Development
Discussions

the observational sensitivity at different pressure levels. When computing the modelled tropospheric columns of NO_2 the tropopause was assumed to be fixed at 100 hPa in the tropics and 250 hPa in the extratropics.

Similarly, when comparing model data with data composites from aircraft campaigns the same period of the year at the same location is selected and mapped into the same grid resolution, 5° x 5° x 1km, before the comparison is made. For some

5   species, the model evaluation is given per seasons: DJF for December-January-February, MAM for March-April-May, JJA for June-July-August and SON for September-October-November.

5.1   Hydroxyl Radical (OH)

One of the means for characterizing the general properties of an AQM is through its ability to simulate OH oxidation. OH is the main oxidant in the troposphere and is responsible for the removal of many compounds, thereby controlling their atmospheric

10   abundance and lifetime. OH is mostly found in the tropical lower and mid troposphere with a strong dependence on the levels of ultraviolet radiation and water vapour. Tropospheric OH formation is mainly due to O_3 photolysis, dominated by the tropics. Also, OH is directly connected to the chemistry of O_3 production since the initial reactions of O_3 formation (VOC+OH and CO+OH) are driven by OH. Hence, O_3 production rates depend on the sources and sinks of odd hydrogen radicals. Primary OH formation also includes the photolysis of HCHO and secondary VOC.

15   The tropospheric mean (air mass weighted) OH derived by the model is 11.5 molec 10^5 cm^{-3}, assuming a tropospheric domain ranging from 200 hPa to the surface. (Note that previous studies suggest that the estimation of the mean OH does not depend on the definition of the tropopause (Voulgarakis et al., 2013).) This value is in good agreement with other studies, e.g., Voulgarakis et al. (2013) where the mean OH concentration from 14 models for 2000 was estimated to be 11.1 ± 1.8 10^5 molec cm^{-3}; Spivakovsky et al. (2000) with 11.6 10^5 molec cm^{-3}, and Prinn et al. (2001) with 9.4 ± 0.13 10^5 molec cm^{-3}.

20   The zonal mean OH concentrations for January, April, July and October 2004 are shown in Fig 2. Seasonal differences reflect the impact of water vapor concentration and stratospheric O_3 column upon incident ultraviolet (UV) radiation (Spivakovsky et al., 2000; Lelieveld et al., 2002). The highest OH concentrations arise in the tropics throughout the year. In northern midlatitudes, the highest OH concentrations are found during summer in the lower to middle troposphere. The latitudinal and seasonal variations are similar to the climatological mean in Spivakovsky et al. (2000), particularly the lower values in the extratropics.

25   Peak concentrations are slightly larger compared to this climatology and other studies (e.g., Horowitz et al., 2003; Huijnen et al., 2010). During January and October the peaks appear in the southern tropics between 700-1000 hPa and 800-1000 hPa, respectively. The peak in April and July is found in the northern tropics between 800-1000 hPa and 700-1000 hPa, respectively. The larger oxidizing capacity compared to other studies could be due to the lack of aerosols in our simulation, which may overestimate photolysis rates in polluted regions.

30   ### 5.2   Carbon monoxide (CO)

CO is one of the most important trace gases in the troposphere exerting a significant influence upon the concentration of oxidants such as OH and O_3 (Wotawa et al., 2001). Main sources of CO in the troposphere are the photochemical production from

the oxidation of hydrocarbons and direct emissions, mainly fossil fuel combustion, biomass burning and biogenic emissions. CO main loss is by reaction with OH, which occurs primarily in the tropics, but also in the extratropics.

In the northern extratropics, the elevated CO concentrations are dominated by anthropogenic emissions and precursor hydrocarbons, which leads to a net CO export to the tropics (Shindell et al., 2006; Bergamaschi et al., 2000). Although most 5 biomass burning occurs in the tropics, gases and aerosols emitted from large wildfires can be transported to the southern extratropics, where emissions and chemical production are lower. Moreover, due to the strong convection, enhanced by forest fire activity, emissions can reach the upper troposphere and the lower stratosphere (Jost et al., 2004; Cammas et al., 2009). CO has a chemical lifetime of a few months ($\sim$1-3), and therefore it is a useful tracer for evaluating transport processes in the model. It is important to keep in mind that despite large Alaskan and Canadian wildfires occurred during the summer, globally 2004 10 had lower CO concentrations than other years during the decade (Elguindi et al., 2010).

An analysis of the CO burden in different regions is presented in Table 6. The global and annual mean burden of CO for 2004 is 399.03 Tg, with higher abundances in the tropics (229.43 Tg CO), followed by the Northern Extratropics (101.71 Tg CO), and the Southern Extratropics (67.88 Tg CO). Other model estimates of the CO burden (Horowitz et al. (2003);Huijnen et al. (2010)) are also shown in Table 6. Our estimates are higher ($\sim$ 46-48 Tg CO) in comparison with these studies in all 15 regions. The largest absolute difference appears in the tropics where the NMMB/BSC-CTM predicts $\sim$ 30-40 Tg CO more than these studies, even though OH is also overestimated. The main sources of CO in the tropics are from biomass burning, biogenic emissions and anthropogenic direct emissions of CO.

We performed tests comparing the annual mean burden of tropospheric CO with and without biomass burning emissions in the model. Neglecting biomass burning emissions only reduced 7% of the tropospheric CO annual mean burden. Therefore, 20 other factors should explain our higher CO burden. On the one side, biogenic emissions are computed online every hour in order to account for evolving meteorological changes, such as solar radiation and surface temperature (see section 2.2.6). Also this simulation neglects the attenuation of radiation due to aerosols, which may produce an overestimation of VOCs biogenic emissions and the derived CO.

The CO anthropogenic emissions used in this study (610.5 Tg/year) are are also higher than those in other inventories (see 25 3.1). The dry deposition of CO is significantly weaker in the NMMB/BSC-CTM (24 Tg CO) than the global model TM5 (184 Tg CO) and the study of Bergamaschi et al. (2000) (292-308 Tg CO). By contrast, other global models such as MOZART-2 have significantly lower dry deposition (2 Tg CO) and the study of Wesely and Hicks (2000) suggests that CO and other relatively inert substances are deposited very slowly. Clearly, there are major uncertainties in the sources and sinks of CO that could be responsible for modeled CO differences.

30 Fig 3 shows the time series of CO daily mean concentration over 14 ground-monitoring stations from the WDCGG database (primarily in the northern mid-latitudes, but with a few of them in the tropics and southern mid-latitudes). The solid red line and the solid black line represent, respectively, the average of observations and the model simulation. Bars show the 25th-75th quartile interval of all observations (orange) and the model simulation (grey). The model is in good agreement with the CO field in the surface layer. However, the model is not able to fully capture the seasonal CO variability, with a slight underestimation 35 during cold months and overestimation during warm months. Such a model limitation could be explained by the fact that most

of the stations are closer to anthropogenic polluted areas, where its concentration is primarily determined by local emissions, and the CO land-based anthropogenic emissions inventory does not have any seasonal variation in this study (see Sec.3.1).

Fig. 4 shows the CO mean bias (MB), correlation and root mean square error for all rural WDCGG stations. The model has a negative MB over stations in Europe and Japan and a positive bias in stations in Canada and Africa, where the correlations are
5   low. The negative bias for several of the northern mid-latitude stations indicates that the higher CO burden found in our model compared to other models in these areas is a feature mainly driven by free tropospheric abundances. Higher correlations are found in northern regions of Europe, southern Africa and eastern Asian countries. Correlation in Canadian stations is between 0.3-0.5. In most of the stations, RMSE is found to be less than 60-40 μg m^{-3}; only 4 stations have an RMSE higher than 60 μg m^{-3}.

10 Additionally, the model was compared with the seasonally averaged vertical profiles of CO from MOZAIC aircraft observations for 2004 in Figs. 5 and S2 in the supplementary information from selected airports: Frankfurt, Beijing, Atlanta, Portland, Abu Zabi and Niamey. The comparison is made only when observations are available; i.e., the same data from the model and the observations are used. Measurements are represented by the solid red line and the model simulation by the solid black line. To understand the variability of the data, standard deviation is plotted in each vertical layer for both model and observations.
15 It is important to note that the number of flights is significantly different between the different airports; therefore, not all comparisons are statistically robust. In addition, note that the scale for Beijing is different (0-1000 ppb) from the others stations (0-400 ppb).

The model captures well the vertical profiles during the first part of the year, with higher biases during the warm months. Generally it overestimates CO from the middle to the upper troposphere in most of the stations throughout the year. Over
20 Frankfurt, the model is in good agreement with the observation during the entire year, despite a slight underestimation during MAM and overestimation during SON in the middle troposphere.

For Beijing, one of the most polluted cities in the world, the model shows a clear tendency to underestimate CO in the lower atmosphere (below 600 hPa). This is probably due to an underestimation in the CO anthropogenic emissions. Most of the AQMs seem to be unable to capture the extreme growth of anthropogenic emissions in China (Akimoto, 2003; Turquety et al.,
25 2008). Over Atlanta, the model performs much better during the winter and spring along the troposphere but positive biases ($\sim$ 20-25 ppb) are seen during the summer and autumn. Regions with biomass burning and biogenic influence, such as Abu Dhabi and Niamey, show a significant overestimation during warm months throughout the tropospheric column. During winter, Stein et al. (2014) also obtain an underestimation of CO vertical profiles in airports located in the Northern Hemisphere (NH).

To complete this CO evaluation, seasonal averages are compared with data from the MOPITT instrument at 800 hPa and 500
30 hPa in Figs. 6 and S3 in the supplementary information, respectively. At 800 hPa, largest differences are seen during boreal winter and spring, where the model clearly overestimates in the tropics and underestimates in the north extratropics and north of Africa. The negative bias during winter ($\sim$ 10-35 ppb) in the NH could further be explained by the lack of a seasonal cycle in anthropogenic emissions. However, the underestimation during NH winter, which appears most state-of-the-art AQMs could also be originated from an underestimation of CO emissions (Stein et al., 2014).

There are significant positive biases over west-central Africa and also over western South America, Indonesia and the surrounding Pacific and Indian oceans during the dry season. Sources of CO over west-central Africa are mainly from biomass burning and biogenic emissions. Uncertainties in the emission inventories have probably contributed to the CO overestimation for these regions. Due to the long-range transport of CO, higher CO concentrations are seen throughout all the year over the tropics and are extended over some parts of the extratropics from June to November. Hence, during JJA and SON the model overestimates CO concentrations in most places including south and central EU and USA ($\sim$ 10-25 ppb).

At 500 hPa, the model presents similar results, with a clear underestimation in the north extratropics and overestimation in the tropics and southern latitudes. Overestimated emissions in Africa or Asia above the PBL can lead to this positive bias in the middle of the troposphere.

Naik et al. (2013) presents an annual average bias of multi-model (17 global models) mean CO for 2000 against average 2000-2006 MOPITT CO at 500 hPa. These models used the same anthropogenic and biomass burning emissions as our study, and a priori and averaging kernels are taken into account for each model before computing biases. The biases in the tropics and extra tropics are similar to those presented here. Hence, these biases might be related to discrepancies in anthropogenic and biomass burning emission inventories, where the magnitude, and perhaps location of emission is not completely understood or correctly modelled. Naik et al. (2013) discussed a too high OH concentration possibly leading to the northern mid-latitude underestimates of CO, which is also a possibility in our case, given the high OH concentrations that the model shows compared to other models. Numerous studies show that the variability in simulated CO among AQMs is large, and uncertainties are diverse including emission's inventories and injection height (Elguindi et al., 2010; Shindell et al., 2006; Prather et al., 2001). A detailed evaluation of MOPITT V4 CO retrievals between 2002-2007 with in situ measurements shows a bias of about -6% at 400 hPa (Deeter et al., 2010). However, this bias is not able to explain the model biases that vary in sign and magnitude between different global regions. Stein et al. (2014) suggests that the persistent negative bias in northern mid-latitude CO in models is most likely due to a combination of too low road traffic emissions and dry deposition errors.

5.3 Nitrogen compounds

The NO$_x$($=$ NO$_2$ + NO) family is one of the key players in the formation of O$_3$ in the troposphere, and during pollution episodes it causes photochemical smog and contributes to acid rain. It has a relatively short lifetime; consequently, it is generally restricted to emission sources, both natural and anthropogenic (mainly fossil fuel combustion). The seasonal cycle of NO$_x$ near the surface is controlled by the seasonality of anthropogenic emissions (especially in the northern hemisphere) and biomass burning emissions (especially in the tropics and the southern Hemisphere). As a result, NO$_x$ is more sensitive to errors in emissions than other pollutants, and errors in NO$_x$ emissions can change NO$_x$ concentrations even more drastically (Miyazaki et al., 2012).

Figure 7 shows the time series of NO$_2$ and NO$_x$ daily mean surface concentrations over 21 and 10 ground-monitoring stations from the EMEP and EANET networks, respectively. In both cases, the model is able to successfully reproduce the seasonal cycle of NO$_2$ and NO$_x$. However, a positive bias is found during the summertime for NO$_2$ in Europe (Fig. 7 top panel). Such a result could be explained by the limitation on the anthropogenic emissions that are constant during the entire

year. Because of that, the model cannot reproduce the decrease in anthropogenic emissions during the summertime, which leads to overestimated concentrations.

Daily profiles show that the modeled NO_2 tends to be too high during nighttime (not shown). This result may be due to the lack of the heterogeneous formation of HNO_3 through N_2O_5 hydrolysis, an important sink of NO_2 at night. In addition, the

5 model does not consider secondary aerosol formation for the present study, which might result in an atmosphere that is too oxidising (overestimation of OH radicals). In combination with the nocturnal chemistry this may lead to an accumulation of NO_2 in the surface layers. However, a slight underestimation is observed between 9-18 UTC. Looking at the annual time series of NO_x in the Asian network (Fig. 7 bottom), it is observed that the model does not reproduce NO_x values, with a sizeable negative bias during the summer. This underestimation could be attributed to an underestimation in the emission inventories,

10 which do not capture the extreme increase of anthropogenic emissions over Asia during the last decade (Akimoto, 2003; Richter et al., 2005), as was the case for CO.

Concerning the spatial statistics (see Fig. 8), the model's prediction capabilities are lower in some regions such as the Iberian Peninsula and most of the stations in Japan, showing poor correlations. The best performance is seen in central EU and stations in Japan that are not in the main island. In general there is a negative bias in most of the stations for these two regions.

15 The comparison of modelled and observed vertical profiles of NO_X, HNO_3 and PAN are presented in Fig. 9 for several regions over US, China, Hawaii and Japan (see Table 5). As explained in Sec. 4.2, the observed vertical profiles do not correspond to the simulated year (see Table 5 for more detail), but the qualitative patterns can provide insights on the model capability to reproduce the chemistry involved. Fig. 9 (first column) shows that vertical profiles of NO_x are in very good agreement with the observed values. The model has a tendency to overestimate NO_X concentrations near the surface; it is

20 likely that NO_X emissions used in this study are higher than the real emissions during the campaigns' periods. Another reason for these higher values over island locations (Japan and Hawaii) could be that emissions are spread throughout the entire low resolution model grid box while the measurements were taken in the cleaner marine boundary layer. In the middle and upper troposphere, the model produces the concentrations well, with a slight underestimation in most of the locations. Note that NO_x lightning emissions are not included in this simulation, which may explain part of this underestimation, particularly in the

25 upper troposphere.

PAN is the main tropospheric reservoir species for NO_x with important implications for the tropospheric O_3 production and the main atmospheric oxidant, OH (Singh and Hanst, 1981). PAN is mainly formed in the boundary layer by oxidation of NMVOCs in the presence of NO_x. NMVOCs and NO_x have both natural and anthropogenic sources. Rapid convection can transport PAN to the middle and upper troposphere and enables the long-range transport of NO_x away from the urban and

30 polluted areas, where it can produce O_3 and OH remotely.

Some features of the vertical profiles are well-captured by the model, although it significantly overestimates PAN concentrations (see Fig. 9, second column). We find overestimations from the surface to the middle atmosphere in Japan, China, Boulder and Churchill, which are possibly explained by an overestimation of biogenic and anthropogenic NO_x surface emissions in this area at surface-level. Another possibility for this overestimation is a too long lifetime for PAN. At most sites, PAN model

35 concentrations tend to increase with altitude, reaching maximum mixing ratios at about 6km, from where they progressively

decrease. This behaviour explains the long thermal decomposition time of PAN (lifetime of approximately a month) and the slow loss by photolysis in the cold middle-upper troposphere. Fischer et al. (2014) analyse the sensitivity of PAN to different emission types, showing that most of the northern hemisphere and Japan are more sensitive to anthropogenic emissions, while the southern hemisphere and the west coast of the USA are more sensitive to biogenic emissions, both contributing to 70-90%

5 of the PAN concentrations.

HNO_3 is mainly produced by the reactions of NO_2 with OH and by the hydrolysis of N_2O_5 on aerosols (we do not account for this reaction in this simulation), and then it is removed by wet and dry deposition. HNO_3 is the main sink of NO_x chemistry. In general, the modelled and observed nitric acid concentrations are in good agreement throughout the troposphere, although the model reveals a tendency to overestimate HNO_3 concentrations that is even more pronounced in US regions. In the regions

10 of Hawaii, Japan and China the model overestimates HNO_3 in the lower-middle troposphere (up to 5km) and underestimates it in the upper troposphere (above 6km). Overestimation of HNO_3 in the troposphere is a common problem in global models (Hauglustaine et al., 1998; Bey et al., 2001; Park et al., 2004; Folberth et al., 2006). HNO_3 concentrations are highly sensitive to the parameterization of wet deposition. One possible reason for this overestimation is that the scavenging from convective precipitation is underestimated.

15 Figure S4 in the supplementary information presents the wet deposition fluxes of HNO_3 in comparison with nitrate observations for three different networks located in Europe, USA and Asia. Satisfactory agreement is found in the HNO_3 wet deposition fluxes with correlations of 0.63 in Europe, 0.80 in USA and 0.52 in Asia. There is a tendency to underestimate in most of the stations, principally in Asia and Europe. Part of this underestimation is because the comparison is between nitric acid (gas) and nitrate (nitric acid + particulate nitrate) wet depositions. However, this tendency to underestimate is consistent

20 with the higher values of HNO_3 observed at the lower and middle troposphere.

Seasonal averages of vertical tropospheric columns (VTC) of NO_2 are compared with SCIAMACHY satellite data in Fig.10. The model is in good agreement with the observations, capturing the high NO_2 values over the most polluted regions, such as Europe, USA and Eastern Asia. The phase in the seasonal cycle of the NO_2 columns is performed well by the model. During the entire year, the model tends to underestimate NO_2 VTCs in big cities, especially during the colder months, and overestimate

25 them in rural regions. The largest discrepancies are seen in eastern China, which suggests an underestimation of emissions regionally. The biomass burning cycle is captured remarkably well, with higher NO_2 VTC in central Africa during DJF and in South America in JJA. Over the sea, the model is in good agreement with SCIAMACHY, showing only small differences ($\pm$ 0.5 $1e^{15}$ molec/cm^2).

5.4 Ozone (O_3)

30 Ozone is one of the central species that drive tropospheric chemistry, and for that reason it is essential that a model reproduces the spatial and temporal concentrations of O_3 well, both at the surface and across the troposphere and stratosphere. O_3 found in the troposphere is originated from in situ photochemical production and from intrusions of O_3 from the stratosphere. O_3 photochemical production in the troposphere involves oxidation of CO and hydrocarbons in the presence of NO_x and sunlight.

In rural areas, CO and CH_4 are the most important species being oxidized in the O_3 formation. However, in polluted areas, short-lived NMVOCs (e.g. HCHO) are present in high concentrations and are the most important species.

The simulated global burden of tropospheric O_3 is shown in Table 7. In the troposphere, O_3 chemical sources and sinks are dominated by the tropics, where high concentrations are found (171.60 Tg O_3). Low concentrations are predicted in the

5   northern extratropics (101.56 Tg O_3) and especially the Southern Extratropics (75.41 Tg O_3), where precursors are not present in high amounts. Similar results are found from other global models, such as MOZART-2 (Horowitz et al., 2003) and TM5 (Huijnen et al., 2010). In general, MOZART-2 has a higher and TM5 a lower annual mean burden of O_3 than the NMMB/BSC-CTM. The annual mean O_3 burden predicted by our model in the southern extratropics is higher (10-14 Tg O_3) than the other two models. Higher CO concentrations in the southern hemisphere (see Table 6) might lead to excessive production of O_3 in

10   this area. In addition, the global tropospheric O_3 burden in our model (348 Tg O_3) is in good agreement with the C-IFS global model (Flemming et al., 2015) and the two multimodel ensemble means of 25 (Stevenson et al., 2006) and 15 (Young et al., 2013) state-of-the-art atmospheric chemistry global models.

According to our calculations, 1209 Tg O_3 are removed from the troposphere by dry deposition at the surface. This quantity is higher in comparison with the global models TM5 (829 Tg O_3) and MOZART-2 (857 Tg O_3). In this sense, the model is

15   in good agreement with the global model LMDz-INCA (1261 Tg O_3) and with the multimodel ensemble study by Stevenson et al. (2006) (1003 $\pm$ 200 Tg O_3). The net stratospheric input, Stratosphere-Troposphere Exchange (STE), annual rate of the model (384 Tg O_3) is also shown in Table 7. The model's STE is in good agreement with other modelling studies, especially with the multimodel ensemble in Stevenson et al. (2006) (552 $\pm$ 168 Tg O_3).

Fig.11 shows the time series of O_3 daily mean concentration averaged over all available monitoring sites (from top to bottom,

20   WDCGG, CASTNET, EMEP and EANET) over the entire simulation period. The solid red line and solid black line represent the average of observations and the model, respectively. Bars show the 25th-75th quartile interval of all observations (orange) and model simulation (grey). As illustrated in Fig.11, there is an overall good performance although there are significant positive bias from May to October in the US and Japan. The seasonal cycle of O_3 from the model agrees well with the observations, showing the highest concentrations during July-August and the lowest concentrations during Nov-Dec over

25   all stations. Although, the model captures the seasonal O_3 variability along this period, there is a tendency to overestimate concentrations during the warmer months, i.e. May-September. This positive bias is significantly higher in the US, where the overestimation occurs all day long (10-20 $\mu g \ m^{-3}$). Over Europe, the overestimation of O_3 levels during summer is lower than in the other regions. Over East Asia the model captures reasonably well the peaks in April and May, although a positive bias is seen during the rest of the year. In this area, concentrations during cold months are overestimated, in contrast to Europe

30   where the model concentrations agree with the observations. Overall the observational networks show a reduction of O_3 concentrations from May-June, but the model has a tendency to simulate an annual cycle with higher concentrations until July. Moreover, a recent study by Val Martin et al. (2014) explains the importance of the dry deposition in controlling surface O_3. Val Martin et al. (2014) shows that accurate dry deposition processes can reduce the summertime surface O_3 bias from 30 ppb to 14 ppb and from 13 ppb to 5 ppb over eastern U.S. and Europe, respectively. Thus, part of this positive bias could be related

to the dry deposition processes included in our model. Further investigation is required to understand model behaviour during this period.

Fig.12 displays the spatial statistics for O_3 over all in-situ monitoring sites using daily mean data. Areas without emissions, such as the south pole and isolated islands in the tropics, have small mean biases and errors and good correlations (>0.80). In polluted areas, a good performance is observed in the US midlands, and parts of central and southern Europe (0.60< r<0.80 and RMSE <20 μg m^{-3}). Large errors are seen in northwestern and southern US and Northern Europe. Although, large errors are seen in all the stations over Japan, the two stations farthest from the main island show high correlation (r> 0.7).

In order to assess the vertical distribution of O_3, the model results are compared with available ozonesondes. The seasonal vertical profiles of O_3 for both the model and observations are compared in Figs.13 and S5 in the supplementary information for the period of study (see Table 3 and Fig. 1 for more details). The comparison is made only when ozonesonde observations are available. Fig.13 and S5 from the supplementary information show (from top to bottom) four panels: DJF, MAM, JJA and SON for each region. Measurements are represented by the solid red line and the model results by the solid black line. The variability of the data is shown in the form of standard deviation for both the model and observations.

The magnitude and vertical profile of O_3 are in good agreement with the observations. However, the model shows a positive bias of $\sim$ 5-20 ppb along the troposphere in most of the regions during the entire year. As shown in Sec. 5.2 there is a significant overestimation of CO, especially in the free troposphere for some regions, which may account for the positive O_3 biases, although the CO overestimation mostly occurs in the tropics where O_3 biases are not so large. Another reason for this result could be that anthropogenic aerosols and secondary aerosol formation are neglected in this simulation, leading to a higher O_3 formation in regions with more precursors. However, this should have more localised effects and therefore it cannot fully explain the biases throughout the troposphere.

The vertical profile is in good agreement with the observations, with O_3 increasing from lower to higher tropospheric layers. In the lower-middle troposphere the model overestimates O_3 in regions with high emissions (Japan, Canada, USA and W.Europe), a feature that is more significant in DJF. In Western Europe and the US, this bias is reduced at the surface level. In tropical areas (Equator, NH tropical and W. Pacific) the model captures well the observed concentration and vertical structure of O_3 in the lower to middle troposphere. However, the model tends to overestimate the O_3 in the vicinity of the tropopause layer in these regions. At polar regions (NH and SH Polar) the model also presents a tendency to overestimate the vertical structure of O_3. O_3 in the tropopause layer is underestimated in the NH Polar case, and overestimated in SH Polar case.

Finally, statistics were computed to identify those areas where the errors are more important. Fig. 14, shows the mean O_3 bias (left), correlation (middle) and RMSE (right) of the model with respect to ozonesondes (data is averaged between 400 and 1000 hPa over the year 2004). As we have shown, the mean bias is positive for most stations (MB<30%). Large RMSE are seen in northern high latitudes (<50 μg m^{-3}) and in two stations from the US. Europe and Japan present an RMSE around 30μg m^{-3} and the tropics and subtropics are regions with lower errors, i.e. RMSE below 30μg m^{-3}. The highest correlations are seen in polar regions.

Geoscientific
Model Development
Discussions

6   Conclusions

A new global chemical transport model, NMMB/BSC-CTM, has been presented. A comprehensive description has been pro-
vided for the different components of the gas-phase chemical module coupled online within the NMMB atmospheric driver.
This model, which includes 51 chemical species and solves 156 reactions, simulates the global distributions of ozone and its
5 precursors, including CO, NO_x, and VOCs. The model simulation presented here is configured with a horizontal resolution
of 1° x 1.4°, with 64 vertical layers and a top of the atmosphere at 1 hPa. Emissions from ACCMIP (Lamarque et al., 2010)
are considered and include fossil fuel combustion, biofuel, biomass burning, soil and oceanic emissions. Biogenic emissions
are calculated online with the MEGANv2.04 model (Guenther et al., 2006). In this simulation, aerosols are neglected, thus, no
interaction between gas-phase and aerosol-phase is considered.

10 Modelled tropospheric ozone and related tracers have been evaluated for the year 2004 and compared with surface-monitoring
stations, ozonesondes, satellite and aircraft campaigns.

The evaluation of OH concentrations shows a good agreement with previous studies (Spivakovsky et al., 2000; Voulgarakis
et al., 2013). The peak concentrations of OH seen in April and July at northern latitudes are slightly higher than the climato-
logical mean calculated in Spivakovsky et al. (2000). This may be possibly explained by the fact that anthropogenic aerosols
15 and secondary aerosol formation are negelcted in this simulation; hence, a higher oxidized atmosphere is obtained due to
higher photolysis when aerosols are not present. However, overall, the widespread positive ozone biases identified seem to be
responsible for the higher OH concentrations.

The global annual mean burden of CO (399 Tg) is higher than in other studies, with larger concentrations located in the
tropics (229.43 Tg CO). The model is in relatively good agreement with CO observations at the surface, and shows negative
20 biases at stations over Europe and Japan, and positive biases in Canada and Africa. The largest correlations are found in
northern Europe, southern Africa and eastern Asia.

Concerning the vertical structure of CO, the model presents a good performance during the DJF and MAM, and positive
biases are seen during JJA for most of the stations. In general, the model overestimates CO from the middle to the upper
troposphere in most of the stations throughout the year. Significant underestimation of CO is seen in Beijing below 600 hPa.
25 This result is similar to other evaluation studies, which indicates that emission inventories are not able to capture the extreme
growth of anthropogenic emissions in China. The phase and amplitude of the seasonal cycles of CO at 800 and 500 hPa in
NMMB/BSC-CTM and MOPITT are quite similar.

Overestimations of CO are mainly located over west-central Africa, western South America, Indonesia and the surrounding
Pacific and Indian oceans during the dry season. At 800 hPa, a significant negative bias is observed over the northern latitudes
30 during winter. These results are most likely related to errors in anthropogenic and biomass burning emission inventories, where
the magnitude and the location of emission are not correctly represented. In addition, CO production from VOCs biogenic
emissions, calculated online and depending on meteorological variables such as radiation, might be overestimated too, due to
the lack of aerosol attenuation of radiation.

Nitrogen oxide abundances are well simulated in almost all locations. Looking at the annual time series of NO_2 in Europe, the model captures the higher peaks during winter, although a positive bias is observed during summer. Nitrogen compounds are more sensitive to errors in emissions than other pollutants. We note that the emission inventory neglects seasonal variations for land-based anthropogenic emissions, and therefore we do not account for the potential reduction of NO_X emissions during

5 summer. Over Asia, there is a negative bias of NO_x from March to August, probably due to underestimated emissions in this area. Vertical profiles of NO_X are in good agreement with the observed values, although there is some underestimation in the upper troposphere, possibly due to the lack of lightning NO_x emissions. Vertical profiles of PAN and HNO_3 were also compared with observations. Some agreement is seen in these vertical profiles, although the model has a tendency to over estimate. HNO_3 wet deposition fluxes tend to be underestimated and are better captured in the US compared to Europe and

10 Asia.

The comparison with observed NO_2 VTC from SCIAMACHY shows that the model reproduces the seasonality and the spatial variability reasonably well, capturing higher NO_2 over the most polluted regions. However, the results show a tendency to underestimate NO_2 VTC in big cities, especially during DJF and SON, possibly due to a low bias in the NO_X emissions. The biomass burning cycle is well captured by the model with higher NO_2 VTC in central Africa during DJF and in South

15 America in JJA.

The ozone burden is in good agreement with other estimates from state-of-the-art global atmospheric chemistry models. The ozone burden in the southern extratropics is higher in our model, suggesting that higher CO concentrations in the southern hemisphere could lead to excessive production of ozone in this area. It seems unlikely that the positive ozone biases are caused by too much STE. STE is in good agreement with other evaluation studies. In addition, STE has stronger effects in the upper

20 troposphere, hence, the related biases should increase with height, which is not the case in our simulations.

The surface O_3 results show a reasonable agreement with the observations, with significant positive biases from May to October in the regions of the US and Japan. Surface O_3 concentrations are very sensitive to the emissions; consequently, the variability of ozone concentrations can be enhanced by improving the spatio-temporal distribution of the ozone precursor emissions.

25 The model captures the spatial and seasonal variation in observed background tropospheric O_3 profiles with a positive bias of $\sim$ 5-20ppb along the troposphere in most of the regions during the whole year. The significant overestimation of CO especially in the free troposphere could be the reason for this positive ozone bias.

In summary, NMMB/BSC-CTM provides a good overall simulation of the main species involved in tropospheric chemistry, although with some caveats that we have highlighted here. Future versions of the model will aim to address problems identified

30 in this study and will include the effect of aerosols in the system.

7 Code Availability

Copies of the code are readily available upon request from the corresponding authors.

Geoscientific
Model Development
Discussions

References

Akimoto, H.: Global air quality and pollution, Science, pp. 1716–1719, 2003.

Arakawa, A.: Computational design for long-term numerical integration of the equations of fluid motion: Two-dimensional incompressible flow. Part I , Journal of Computational Physics, 1, 119 – 143, doi:http://dx.doi.org/10.1016/0021-9991(66)90015-5, http://www.sciencedirect.com/science/article/pii/0021999166900155, 1966.

Ashworth, K., Wild, O., and Hewitt, C. N.: Sensitivity of isoprene emissions estimated using MEGAN to the time resolution of input climate data, Atmospheric Chemistry and Physics, 10, 1193–1201, doi:10.5194/acp-10-1193-2010, http://www.atmos-chem-phys.net/10/1193/2010/, 2010.

Atkinson, R., Baulch, D. L., Cox, R. A., Crowley, J. N., Hampson, R. F., Hynes, R. G., Jenkin, M. E., Rossi, M. J., and Troe, J.: Evaluated kinetic and photochemical data for atmospheric chemistry: Volume I - gas phase reactions of O_x, HO_x, NO_x and SO_x species, Atmospheric Chemistry and Physics, 4, 1461–1738, doi:10.5194/acp-4-1461-2004, http://www.atmos-chem-phys.net/4/1461/2004/, 2004.

Atlas, E. L., Ridley, B. A., and Cantrell, C. A.: The Tropospheric Ozone Production about the Spring Equinox (TOPSE) Experiment: Introduction, Journal of Geophysical Research: Atmospheres, 108, doi:10.1029/2002JD003172, http://dx.doi.org/10.1029/2002JD003172, 2003.

Badia, A. and Jorba, O.: Gas-phase evaluation of the online NMMB/BSC-CTM model over Europe for 2010 in the framework of the AQMEII-Phase2 project, Atmospheric Environment, doi:http://dx.doi.org/10.1016/j.atmosenv.2014.05.055, http://www.sciencedirect.com/science/article/pii/S1352231014004026, 2014.

Baklanov, A., Schlünzen, K., Suppan, P., Baldasano, J., Brunner, D., Aksoyoglu, S., Carmichael, G., Douros, J., Flemming, J., Forkel, R., Galmarini, S., Gauss, M., Grell, G., Hirtl, M., Joffre, S., Jorba, O., Kaas, E., Kaasik, M., Kallos, G., Kong, X., Korsholm, U., Kurganskiy, A., Kushta, J., Lohmann, U., Mahura, A., Manders-Groot, A., Maurizi, A., Moussiopoulos, N., Rao, S. T., Savage, N., Seigneur, C., Sokhi, R. S., Solazzo, E., Solomos, S., Sørensen, B., Tsegas, G., Vignati, E., Vogel, B., and Zhang, Y.: Online coupled regional meteorology chemistry models in Europe: current status and prospects, Atmospheric Chemistry and Physics, 14, 317–398, doi:10.5194/acp-14-317-2014, http://www.atmos-chem-phys.net/14/317/2014/, 2014.

Bergamaschi, P., Hein, R., Heimann, M., and Crutzen, P. J.: Inverse modeling of the global CO cycle: 1. Inversion of CO mixing ratios, Journal of Geophysical Research: Atmospheres, 105, 1909–1927, doi:10.1029/1999JD900818, http://dx.doi.org/10.1029/1999JD900818, 2000.

Betts, A. K.: A new convective adjustment scheme. Part I: Observational and theoretical basis, Quarterly Journal of the Royal Meteorological Society, 112, 677–691, doi:10.1002/qj.49711247307, http://dx.doi.org/10.1002/qj.49711247307, 1986.

Betts, A. K. and Miller, M. J.: A new convective adjustment scheme. Part II: Single column tests using GATE wave, BOMEX, ATEX and arctic air-mass data sets, Quarterly Journal of the Royal Meteorological Society, 112, 693–709, doi:10.1002/qj.49711247308, http://dx.doi.org/10.1002/qj.49711247308, 1986.

Bey, I., Jacob, D. J., Yantosca, R. M., Logan, J. A., Field, B. D., Fiore, A. M., Li, Q., Liu, H. Y., Mickley, L. J., and Schultz, M. G.: Global modeling of tropospheric chemistry with assimilated meteorology: Model description and evaluation, Journal of Geophysical Research: Atmospheres, 106, 23 073–23 095, doi:10.1029/2001JD000807, http://dx.doi.org/10.1029/2001JD000807, 2001.

Boersma, K. F., Eskes, H. J., and Brinksma, E. J.: Error analysis for tropospheric NO2 retrieval from space, Journal of Geophysical Research: Atmospheres, 109, n/a–n/a, doi:10.1029/2003JD003962, http://dx.doi.org/10.1029/2003JD003962, 2004.

Geoscientific
Model Development
Discussions

Byun, D.: Fundamentals of one-atmosphere dynamics for multiscale Air Quality Modeling, Tech. rep., EPA/600/R-99/030, http://www.epa.gov/AMD/CMAQ/ch05.pdf, 1990.

Byun, D. and Ching, J.: Science algorithms of the EPA Models-3 community multiscale air quality (CMAQ) modeling system, Rep. EPA/600/R-99, 30, 1999.

5   Cammas, J.-P., Brioude, J., Chaboureau, J.-P., Duron, J., Mari, C., Mascart, P., Nédélec, P., Smit, H., Pätz, H.-W., Volz-Thomas, A., Stohl, A., and Fromm, M.: Injection in the lower stratosphere of biomass fire emissions followed by long-range transport: a MOZAIC case study, Atmospheric Chemistry and Physics, 9, 5829–5846, doi:10.5194/acp-9-5829-2009, http://www.atmos-chem-phys.net/9/5829/2009/, 2009.

Cariolle, D. and Déqué, M.: Southern hemisphere medium-scale waves and total ozone disturbances in a spectral general circulation model, Journal of Geophysical Research: Atmospheres, 91, 10 825–10 846, doi:10.1029/JD091iD10p10825, http://dx.doi.org/10.1029/JD091iD10p10825, 1986.

10 Chang, J. S., Brost, R. A., Isaksen, I. S. A., Madronich, S., Middleton, P., Stockwell, W. R., and Walcek, C. J.: A three-dimensional Eulerian acid deposition model: Physical concepts and formulation, Journal of Geophysical Research: Atmospheres, 92, 14 681–14 700, doi:10.1029/JD092iD12p14681, http://dx.doi.org/10.1029/JD092iD12p14681, 1987.

Chipperfield, M. P.: New version of the TOMCAT/SLIMCAT off-line chemical transport model: Intercomparison of stratospheric tracer
15 experiments, Quarterly Journal of the Royal Meteorological Society, 132, 1179–1203, doi:10.1256/qj.05.51, http://dx.doi.org/10.1256/qj.05.51, 2006.

Crutzen, P. J.: Photochemical reactions initiated by and influencing ozone in unpolluted tropospheric air, Tellus, 26, 47–57, doi:10.1111/j.2153-3490.1974.tb01951.x, http://dx.doi.org/10.1111/j.2153-3490.1974.tb01951.x, 1974.

Damian, V., Sandu, A., Damian, M., Potra, F., and Carmichael, G. R.: The kinetic preprocessor KPP-a software environment for solving
20 chemical kinetics , Computers and Chemical Engineering, 26, 1567 – 1579, doi:http://dx.doi.org/10.1016/S0098-1354(02)00128-X, http://www.sciencedirect.com/science/article/pii/S009813540200128X, 2002.

Deeter, M. N., Edwards, D. P., Gille, J. C., Emmons, L. K., Francis, G., Ho, S.-P., Mao, D., Masters, D., Worden, H., Drummond, J. R., and Novelli, P. C.: The MOPITT version 4 CO product: Algorithm enhancements, validation, and long-term stability, Journal of Geophysical Research: Atmospheres, 115, n/a–n/a, doi:10.1029/2009JD013005, http://dx.doi.org/10.1029/2009JD013005, 2010.

25 Deeter, M. N., Martinez-Alonso, S., Edwards, D. P., Emmons, L. K., Gille, J. C., Worden, H. M., Pittman, J. V., Daube, B. C., and Wofsy, S. C.: Validation of MOPITT Version 5 thermal-infrared, near-infrared, and multispectral carbon monoxide profile retrievals for 2000-2011, Journal of Geophysical Research: Atmospheres, 118, 6710–6725, doi:10.1002/jgrd.50272, http://dx.doi.org/10.1002/jgrd.50272, 2013.

Derwent, R., Jenkin, M., and Saunders, S.: Photochemical ozone creation potentials for a large number of reactive hydrocarbons un-
30 der European conditions, Atmospheric Environment, 30, 181 – 199, doi:http://dx.doi.org/10.1016/1352-2310(95)00303-G, http://www.sciencedirect.com/science/article/pii/135223109500303G, 1996.

Ek, M. B., Mitchell, K. E., Lin, Y., Rogers, E., Grunmann, P., Koren, V., Gayno, G., and Tarpley, J. D.: Implementation of Noah land surface model advances in the National Centers for Environmental Prediction operational mesoscale Eta model, Journal of Geophysical Research: Atmospheres, 108, n/a–n/a, doi:10.1029/2002JD003296, http://dx.doi.org/10.1029/2002JD003296, 2003.

35 Elguindi, N., Clark, H., Ordóñez, C., Thouret, V., Flemming, J., Stein, O., Huijnen, V., Moinat, P., Inness, A., Peuch, V.-H., Stohl, A., Turquety, S., Athier, G., Cammas, J.-P., and Schultz, M.: Current status of the ability of the GEMS/MACC models to reproduce the tropospheric CO vertical distribution as measured by MOZAIC, Geoscientific Model Development, 3, 501–518, doi:10.5194/gmd-3-501-2010, http://www.geosci-model-dev.net/3/501/2010/, 2010.

Emmons, L. K., Hauglustaine, D. A., Müller, J.-F., Carroll, M. A., Brasseur, G. P., Brunner, D., Staehelin, J., Thouret, V., and Marenco, A.:
Data composites of airborne observations of tropospheric ozone and its precursors, Journal of Geophysical Research: Atmospheres, 105,
20 497–20 538, doi:10.1029/2000JD900232, http://dx.doi.org/10.1029/2000JD900232, 2000.

Emmons, L. K., Hess, P., Klonecki, A., Tie, X., Horowitz, L., Lamarque, J.-F., Kinnison, D., Brasseur, G., Atlas, E., Browell, E., Cantrell,
5   C., Eisele, F., Mauldin, R. L., Merrill, J., Ridley, B., and Shetter, R.: Budget of tropospheric ozone during TOPSE from two chemical
transport models, Journal of Geophysical Research: Atmospheres, 108, n/a–n/a, doi:10.1029/2002JD002665, http://dx.doi.org/10.1029/
2002JD002665, 2003.

Emmons, L. K., Walters, S., Hess, P. G., Lamarque, J.-F., Pfister, G. G., Fillmore, D., Granier, C., Guenther, A., Kinnison, D., Laepple,
T., Orlando, J., Tie, X., Tyndall, G., Wiedinmyer, C., Baughcum, S. L., and Kloster, S.: Description and evaluation of the Model for
10   Ozone and Related chemical Tracers, version 4 (MOZART-4), Geoscientific Model Development, 3, 43–67, doi:10.5194/gmd-3-43-2010,
http://www.geosci-model-dev.net/3/43/2010/, 2010.

Fast, J. D., Gustafson, W. I., Easter, R. C., Zaveri, R. A., Barnard, J. C., Chapman, E. G., Grell, G. A., and Peckham, S. E.: Evolution of ozone,
particulates, and aerosol direct radiative forcing in the vicinity of Houston using a fully coupled meteorology-chemistry-aerosol model,
Journal of Geophysical Research: Atmospheres, 111, n/a–n/a, doi:10.1029/2005JD006721, http://dx.doi.org/10.1029/2005JD006721,
15   2006.

Fels, S. B. and Schwarzkopf, M. D.: The Simplified Exchange Approximation: A New Method for Radiative Transfer Calculations, J.
Atmos. Sci., 32, 1475–1488, doi:10.1175/1520-0469(1975)032<1475:TSEAAN>2.0.CO;2, http://dx.doi.org/10.1175/1520-0469(1975)
032<1475:TSEAAN>2.0.CO;2, 1975.

Ferrier, B. S., Y., J., Y., L., T., B., E., R., and G., D.: Implementation of a new grid-scale cloud and precipitation scheme in the NCEP Eta
20   model, paper presented at 15th Conference on Numerical Weather Prediction, Am. Meteorol. Soc., San Antonio, Tex., 2002.

Fischer, E. V., Jacob, D. J., Yantosca, R. M., Sulprizio, M. P., Millet, D. B., Mao, J., Paulot, F., Singh, H. B., Roiger, A., Ries, L., Talbot,
R., Dzepina, K., and Pandey Deolal, S.: Atmospheric peroxyacetyl nitrate (PAN): a global budget and source attribution, Atmospheric
Chemistry and Physics, 14, 2679–2698, doi:10.5194/acp-14-2679-2014, http://www.atmos-chem-phys.net/14/2679/2014/, 2014.

Flemming, J., Huijnen, V., Arteta, J., Bechtold, P., Beljaars, A., Blechschmidt, A.-M., Diamantakis, M., Engelen, R. J., Gaudel, A., Inness,
25   A., Jones, L., Josse, B., Katragkou, E., Marecal, V., Peuch, V.-H., Richter, A., Schultz, M. G., Stein, O., and Tsikerdekis, A.: Tropospheric
chemistry in the Integrated Forecasting System of ECMWF, Geoscientific Model Development, 8, 975–1003, doi:10.5194/gmd-8-975-
2015, http://www.geosci-model-dev.net/8/975/2015/, 2015.

Folberth, G. A., Hauglustaine, D. A., Lathière, J., and Brocheton, F.: Interactive chemistry in the Laboratoire de Météorologie Dynamique
general circulation model: model description and impact analysis of biogenic hydrocarbons on tropospheric chemistry, Atmospheric
30   Chemistry and Physics, 6, 2273–2319, doi:10.5194/acp-6-2273-2006, http://www.atmos-chem-phys.net/6/2273/2006/, 2006.

Foley, K. M., Roselle, S. J., Appel, K. W., Bhave, P. V., Pleim, J. E., Otte, T. L., Mathur, R., Sarwar, G., Young, J. O., Gilliam, R. C., Nolte,
C. G., Kelly, J. T., Gilliland, A. B., and Bash, J. O.: Incremental testing of the Community Multiscale Air Quality (CMAQ) modeling
system version 4.7, Geoscientific Model Development, 3, 205–226, doi:10.5194/gmd-3-205-2010, http://www.geosci-model-dev.net/3/
205/2010/, 2010.

35   Gery, M. W., Whitten, G. Z., Killus, J. P., and Dodge, M. C.: A photochemical kinetics mechanism for urban and regional scale computer
modeling, Journal of Geophysical Research: Atmospheres, 94, 12 925–12 956, doi:10.1029/JD094iD10p12925, http://dx.doi.org/10.1029/
JD094iD10p12925, 1989.

Geoscientific
Model Development
Discussions

Gong, S. L., Lavoué, D., Zhao, T. L., Huang, P., and Kaminski, J. W.: GEM-AQ/EC, an on-line global multi-scale chemical weather mod-
elling system: model development and evaluation of global aerosol climatology, Atmospheric Chemistry and Physics, 12, 8237–8256,
doi:10.5194/acp-12-8237-2012, http://www.atmos-chem-phys.net/12/8237/2012/, 2012.

Granier, C., Lamarque, J., Mieville, A., Muller, J., Olivier, J., Orlando, J., Peters, J., Petron, G., Tyndall, G., and Wallens, S.: POET, a
5   database of surface emissions of ozone precursors, http://www. aero. jussieu. fr/projet/ACCENT/POET. php, 6988, 30, 2005.

Guenther, A., Karl, T., Harley, P., Wiedinmyer, C., Palmer, P. I., and Geron, C.: Estimates of global terrestrial isoprene emissions using
MEGAN (Model of Emissions of Gases and Aerosols from Nature), Atmospheric Chemistry and Physics, 6, 3181–3210, doi:10.5194/acp-
6-3181-2006, http://www.atmos-chem-phys.net/6/3181/2006/, 2006.

Hauglustaine, D. A., Brasseur, G. P., Walters, S., Rasch, P. J., Müller, J.-F., Emmons, L. K., and Carroll, M. A.: MOZART, a global chemical
10   transport model for ozone and related chemical tracers: 2. Model results and evaluation, Journal of Geophysical Research: Atmospheres,
103, 28 291–28 335, doi:10.1029/98JD02398, http://dx.doi.org/10.1029/98JD02398, 1998.

Haustein, K., Pérez, C., Baldasano, J. M., Jorba, O., S., B., Miller, R., Janjic, Z., Black, T., Nickovic, S., Todd, M., and Washington, R.:
Atmospheric dust modeling from meso to global scales with the online NMMB/BSC-Dust model - Part 2: Experimental campaigns in
Northern Africa, Atmos. Chem. Phys., 12, 2933–2958, doi:10.5194/acp-12-2933-2012., 2012.

15   Hertel, O., Berkowicz, R., Christensen, J., and Øystein Hov: Test of two numerical schemes for use in atmospheric transport-chemistry
models , Atmospheric Environment. Part A. General Topics, 27, 2591 – 2611, doi:http://dx.doi.org/10.1016/0960-1686(93)90032-T, http:
//www.sciencedirect.com/science/article/pii/096016869390032T, 1993.

Heue, K.-P., Richter, A., Bruns, M., Burrows, J. P., v. Friedeburg, C., Platt, U., Pundt, I., Wang, P., and Wagner, T.: Validation of
SCIAMACHY tropospheric NO_2-columns with AMAXDOAS measurements, Atmospheric Chemistry and Physics, 5, 1039–1051,
20   doi:10.5194/acp-5-1039-2005, http://www.atmos-chem-phys.net/5/1039/2005/, 2005.

Hilboll, A., Richter, A., Rozanov, A., Hodnebrog, Ø., Heckel, A., Solberg, S., Stordal, F., and Burrows, J. P.: Improvements to the retrieval
of tropospheric NO2 from satellite–stratospheric correction using SCIAMACHY limb/nadir matching and comparison to Oslo CTM2
simulations, Atmospheric Measurement Techniques, 6, 565–584, doi:10.5194/amt-6-565-2013, http://www.atmos-meas-tech.net/6/565/
2013/, 2013.

25   Horowitz, L. W., Walters, S., Mauzerall, D. L., Emmons, L. K., Rasch, P. J., Granier, C., Tie, X., Lamarque, J.-F., Schultz, M. G., Tyndall,
G. S., Orlando, J. J., and Brasseur, G. P.: A global simulation of tropospheric ozone and related tracers: Description and evaluation
of MOZART, version 2, Journal of Geophysical Research: Atmospheres, 108, doi:10.1029/2002JD002853, http://dx.doi.org/10.1029/
2002JD002853, 2003.

Hsu, J. and Prather, M. J.: Stratospheric variability and tropospheric ozone, Journal of Geophysical Research: Atmospheres, 114,
30   doi:10.1029/2008JD010942, http://dx.doi.org/10.1029/2008JD010942, 2009.

Huijnen, V., Williams, J., van Weele, M., van Noije, T., Krol, M., Dentener, F., Segers, A., Houweling, S., Peters, W., de Laat, J., Boersma,
F., Bergamaschi, P., van Velthoven, P., Le Sager, P., Eskes, H., Alkemade, F., Scheele, R., Nédélec, P., and Pätz, H.: The global chemistry
transport model TM5: description and evaluation of the tropospheric chemistry version 3.0, Geoscientific Model Development, 3, 445–
473, doi:10.5194/gmd-3-445-2010, http://www.geosci-model-dev.net/3/445/2010/, 2010.

35   Im, U., Bianconi, R., Solazzo, E., Kioutsioukis, I., Badia, A., Balzarini, A., Baró, R., Bellasio, R., Brunner, D., Chemel, C., Curci, G.,
Flemming, J., Forkel, R., Giordano, L., Jiménez-Guerrero, P., Hirtl, M., Hodzic, A., Honzak, L., Jorba, O., Knote, C., Kuenen, J., Makar,
P., Manders-Groot, A., Neal, L., Pérez, J., Pirovano, G., Pouliot, G. San Jose, R., Savage, N., Schroder, W., Sokhi, R., Syrakov, D., Torian,
A., Tuccella, R., Werhahn, J., Wolke, R., Yahya, K., Zabkar, R., Zhang, Y., Zhang, J., Hogrefe, C., and Galmarini, S.: Evaluation of

Geoscientific
Model Development
Discussions

EGU
Open Access

operational online-coupled regional air quality models over Europe and North America in the context of AQMEII phase 2. Part I: Ozone, Atmospheric Environment, pp. –, doi:http://dx.doi.org/10.1016/j.atmosenv.2014.09.042, http://www.sciencedirect.com/science/article/pii/S1352231014007353, 2014.

Inness, A., Baier, F., Benedetti, A., Bouarar, I., Chabrillat, S., Clark, H., Clerbaux, C., Coheur, P., Engelen, R. J., Errera, Q., Flemming, J., George, M., Granier, C., Hadji-Lazaro, J., Huijnen, V., Hurtmans, D., Jones, L., Kaiser, J. W., Kapsomenakis, J., Lefever, K., Leitão, J., Razinger, M., Richter, A., Schultz, M. G., Simmons, A. J., Suttie, M., Stein, O., Thépaut, J.-N., Thouret, V., Vrekoussis, M., Zerefos, C., and the MACC team: The MACC reanalysis: an 8 yr data set of atmospheric composition, Atmospheric Chemistry and Physics, 13, 4073–4109, doi:10.5194/acp-13-4073-2013, http://www.atmos-chem-phys.net/13/4073/2013/, 2013.

Jacob, D. J., Crawford, J. H., Kleb, M. M., Connors, V. S., Bendura, R. J., Raper, J. L., Sachse, G. W., Gille, J. C., Emmons, L., and Heald, C. L.: Transport and Chemical Evolution over the Pacific (TRACE-P) aircraft mission: Design, execution, and first results, Journal of Geophysical Research: Atmospheres, 108, n/a–n/a, doi:10.1029/2002JD003276, http://dx.doi.org/10.1029/2002JD003276, 2003.

Jacobson, M. Z.: GATOR-GCMM: A global- through urban-scale air pollution and weather forecast model: 1. Model design and treatment of subgrid soil, vegetation, roads, rooftops, water, sea ice, and snow, Journal of Geophysical Research: Atmospheres, 106, 5385–5401, doi:10.1029/2000JD900560, http://dx.doi.org/10.1029/2000JD900560, 2001.

Janjic, Z.: Pressure gradient force and advection scheme used for forecasting with steep and small scale topography, Contrib. Atmos. Phys., 50, 186–199., 1977.

Janjic, Z.: Forward–backward scheme modified to prevent two–grid–interval noise and its application in sigma coordinate models., Contrib. Atmos. Phys., 52, 69–84, 1979.

Janjic, Z.: Nonlinear Advection Schemes and Energy Cascade on Semi-Staggered Grids, 112, 1234–1245, doi:doi: 10.1175/1520-0493(1984)112<1234:NASAEC>2.0.CO;2, http://dx.doi.org/10.1175/1520-0493(1984)112<1234:NASAEC>2.0.CO;2, 1984.

Janjic, Z.: The step-mountain coordinates: physical package., Monthly Weather Review, 118, 1429–1443, doi:10.1175/1520-0493(1990)118<1429:TSMCPP>2.0.CO;2, http://dx.doi.org/10.1175/1520-0493(1990)118<1429:TSMCPP>2.0.CO;2, 1990.

Janjic, Z.: The Step-Mountain Eta Coordinate Model: Further Developments of the Convection, Viscous Sublayer, and Turbulence Closure Schemes, Monthly Weather Review, 122, 1994.

Janjic, Z.: Comments on Development and Evaluation of a Convection Scheme for Use in Climate Models, Journal of the Atmospheric Sciences, 57, 3686–3686, 2000.

Janjic, Z.: A nonhydrostatic model based on a new approach, Meteorology and Atmospheric Physics, 82, 271–285, 2003.

Janjic, Z. and Black, T.: A unified model approach from meso to global scales, 7, 24–29, http://meetings.copernicus.org/www.cosis.net/abstracts/EGU05/05582/EGU05-J-05582.pdf, 2005.

Janjic, Z. and Gall, I.: Scientific documentation of the NCEP nonhydrostatic multiscale model on the B grid (NMMB). Part 1 Dynamics, Tech. rep., Tech. rep., NCAR/TN-489+STR, doi:http://dx.doi.org/10.5065/D6WH2MZX10.5065/D6WH2MZX, http://nldr.library.ucar.edu/repository/collections/TECH-NOTE-000-000-000-857, 2012.

Janjic, Z., Gerrity Jr., J., and Nickovic, S.: An alternative approach to nonhydrostatic modeling, Monthly Weather Review, 129, 1164–1178, 2001.

Janjic, Z., Huang, H., and Lu, S.: A unified atmospheric model suitable for studying transport of mineral aerosols from meso to global scales, in: IOP Conference Series: Earth and Environmental Science, vol. 7, p. 012011, IOP Publishing, 2009.

Geoscientific
Model Development
Discussions

Jorba, O., Dabdub, D., Blaszczak-Boxe, C., Pérez, C., Janjic, Z., Baldasano, J. M., Spada, M., Badia, A., and Gonçalves, M.: Potential significance of photoexcited NO_2 on global air quality with the NMMB/BSC chemical transport model, Journal of Geophysical Research: Atmospheres, 117, doi:10.1029/2012JD017730, http://dx.doi.org/10.1029/2012JD017730, 2012.

Jost, H.-J., Drdla, K., Stohl, A., Pfister, L., Loewenstein, M., Lopez, J. P., Hudson, P. K., Murphy, D. M., Cziczo, D. J., Fromm, M., Bui, T. P., Dean-Day, J., Gerbig, C., Mahoney, M. J., Richard, E. C., Spichtinger, N., Pittman, J. V., Weinstock, E. M., Wilson, J. C., and Xueref, I.: In-situ observations of mid-latitude forest fire plumes deep in the stratosphere, Geophysical Research Letters, 31, n/a–n/a, doi:10.1029/2003GL019253, http://dx.doi.org/10.1029/2003GL019253, 2004.

Lamarque, J.-F., Bond, T. C., Eyring, V., Granier, C., Heil, A., Klimont, Z., Lee, D., Liousse, C., Mieville, A., Owen, B., Schultz, M. G., Shindell, D., Smith, S. J., Stehfest, E., Van Aardenne, J., Cooper, O. R., Kainuma, M., Mahowald, N., McConnell, J. R., Naik, V., Riahi, K., and van Vuuren, D. P.: Historical (1850–2000) gridded anthropogenic and biomass burning emissions of reactive gases and aerosols: methodology and application, Atmospheric Chemistry and Physics, 10, 7017–7039, doi:10.5194/acp-10-7017-2010, http://www.atmos-chem-phys.net/10/7017/2010/, 2010.

Lamarque, J.-F., Shindell, D. T., Josse, B., Young, P. J., Cionni, I., Eyring, V., Bergmann, D., Cameron-Smith, P., Collins, W. J., Doherty, R., Dalsoren, S., Faluvegi, G., Folberth, G., Ghan, S. J., Horowitz, L. W., Lee, Y. H., MacKenzie, I. A., Nagashima, T., Naik, V., Plummer, D., Righi, M., Rumbold, S. T., Schulz, M., Skeie, R. B., Stevenson, D. S., Strode, S., Sudo, K., Szopa, S., Voulgarakis, A., and Zeng, G.: The Atmospheric Chemistry and Climate Model Intercomparison Project (ACCMIP): overview and description of models, simulations and climate diagnostics, Geoscientific Model Development, 6, 179–206, doi:10.5194/gmd-6-179-2013, http://www.geosci-model-dev.net/6/179/2013/, 2013.

Lelieveld, J., Peters, W., Dentener, F. J., and Krol, M. C.: Stability of tropospheric hydroxyl chemistry, Journal of Geophysical Research: Atmospheres, 107, ACH 17–1–ACH 17–11, doi:10.1029/2002JD002272, http://dx.doi.org/10.1029/2002JD002272, 2002.

Marais, E. A., Jacob, D. J., Guenther, A., Chance, K., Kurosu, T. P., Murphy, J. G., Reeves, C. E., and Pye, H. O. T.: Improved model of isoprene emissions in Africa using Ozone Monitoring Instrument (OMI) satellite observations of formaldehyde: implications for oxidants and particulate matter, Atmospheric Chemistry and Physics, 14, 7693–7703, doi:10.5194/acp-14-7693-2014, http://www.atmos-chem-phys.net/14/7693/2014/, 2014.

Miyazaki, K., Eskes, H. J., and Sudo, K.: Global NO_x emission estimates derived from an assimilation of OMI tropospheric NO_2 columns, Atmospheric Chemistry and Physics, 12, 2263–2288, doi:10.5194/acp-12-2263-2012, http://www.atmos-chem-phys.net/12/2263/2012/, 2012.

Mlawer, E. J., Taubman, S. J., Brown, P. D., Iacono, M. J., and Clough, S. A.: Radiative transfer for inhomogeneous atmospheres: RRTM, a validated correlated-k model for the longwave, Journal of Geophysical Research: Atmospheres, 102, 16663–16682, doi:10.1029/97JD00237, http://dx.doi.org/10.1029/97JD00237, 1997.

Monge-Sanz, B. M., Chipperfield, M. P., Cariolle, D., and Feng, W.: Results from a new linear O_3 scheme with embedded heterogeneous chemistry compared with the parent full-chemistry 3-D CTM, Atmospheric Chemistry and Physics, 11, 1227–1242, doi:10.5194/acp-11-1227-2011, http://www.atmos-chem-phys.net/11/1227/2011/, 2011.

Monin, A. S. and Obukhov, A. M.: Osnovnye zakonomernosti turbulentnogo peremesivanija v prizemnom sloe atmosfery, Trudy geofiz. inst. AN SSSR, 24 (151), 163–187, 1954.

Naik, V., Voulgarakis, A., Fiore, A. M., Horowitz, L. W., Lamarque, J.-F., Lin, M., Prather, M. J., Young, P. J., Bergmann, D., Cameron-Smith, P. J., Cionni, I., Collins, W. J., Dalsøren, S. B., Doherty, R., Eyring, V., Faluvegi, G., Folberth, G. A., Josse, B., Lee, Y. H., MacKenzie, I. A., Nagashima, T., van Noije, T. P. C., Plummer, D. A., Righi, M., Rumbold, S. T., Skeie, R., Shindell, D. T., Stevenson, D. S., Strode,

S., Sudo, K., Szopa, S., and Zeng, G.: Preindustrial to present-day changes in tropospheric hydroxyl radical and methane lifetime from the Atmospheric Chemistry and Climate Model Intercomparison Project (ACCMIP), Atmospheric Chemistry and Physics, 13, 5277–5298, doi:10.5194/acp-13-5277-2013, http://www.atmos-chem-phys.net/13/5277/2013/, 2013.

Park, R. J., Pickering, K. E., Allen, D. J., Stenchikov, G. L., and Fox-Rabinovitz, M. S.: Global simulation of tropospheric ozone using the University of Maryland Chemical Transport Model (UMD-CTM): 1. Model description and evaluation, Journal of Geophysical Research: Atmospheres, 109, n/a–n/a, doi:10.1029/2003JD004266, http://dx.doi.org/10.1029/2003JD004266, 2004.

Pérez, C., Haustein, K., Janjic, Z., Jorba, O., Huneeus, N., Baldasano, J. M., Black, T., Basart, S., Nickovic, S., Miller, R. L., Perlwitz, J. P., Schulz, M., and Thomson, M.: Atmospheric dust modeling from meso to global scales with the online NMMB/BSC-Dust model Part 1: Model description, annual simulations and evaluation, Atmospheric Chemistry and Physics, 11, 13 001–13 027, doi:10.5194/acp-11-13001-2011, http://www.atmos-chem-phys.net/11/13001/2011/, 2011.

Petritoli, A., Bonasoni, P., Giovanelli, G., Ravegnani, F., Kostadinov, I., Bortoli, D., Weiss, A., Schaub, D., Richter, A., and Fortezza, F.: First comparison between ground-based and satellite-borne measurements of tropospheric nitrogen dioxide in the Po basin, Journal of Geophysical Research: Atmospheres, 109, n/a–n/a, doi:10.1029/2004JD004547, http://dx.doi.org/10.1029/2004JD004547, 2004.

Prather, M., Ehhalt, D., and Dentener, F.: Atmospheric chemistry and greenhouse gases in Climate Change 2001, 2001.

Prinn, R., Huang, J., Weiss, R., Cunnold, D., Fraser, P., Simmonds, P., McCulloch, A., Harth, C., Salameh, P., O'Doherty, S., Wang, R., Porter, L., and Miller, B.: Evidence for substantial variations of atmospheric hydroxyl radicals in the past two decades, Science, 292, 1882–1888, http://www.sciencemag.org/content/292/5523/1882, 2001.

Richter, A., Burrows, J. P., Nüß, H., Granier, C., and Niemeier, U.: Increase in tropospheric nitrogen dioxide over China observed from space, Nature, 437, 129–132, 2005.

Sander, S. P., Golden, D., Kurylo, M., Moortgat, G., Wine, P., Ravishankara, A., Kolb, C., Molina, M., Finlayson-Pitts, B., Huie, R., et al.: Chemical kinetics and photochemical data for use in atmospheric studies evaluation number 15, 2006.

Sandu, A. and Sander, R.: Technical note: Simulating chemical systems in Fortran90 and Matlab with the Kinetic PreProcessor KPP-2.1, Atmospheric Chemistry and Physics, 6, 187–195, doi:10.5194/acp-6-187-2006, http://www.atmos-chem-phys.net/6/187/2006/, 2006.

Schultz, M. and Rast, S.: Emission datasets and methodologies for estimating emissions , Tech. rep., RETRO Report D1-6, http://retro.enes.org, 2007.

Seinfeld, J. and Pandis, S.: Atmospheric Chemistry and Physics, Wiley-Interscience, New York., 1998.

Shindell, D. T., Faluvegi, G., Stevenson, D. S., Krol, M. C., Emmons, L. K., Lamarque, J.-F., Pétron, G., Dentener, F. J., Ellingsen, K., Schultz, M. G., Wild, O., Amann, M., Atherton, C. S., Bergmann, D. J., Bey, I., Butler, T., Cofala, J., Collins, W. J., Derwent, R. G., Doherty, R. M., Drevet, J., Eskes, H. J., Fiore, A. M., Gauss, M., Hauglustaine, D. A., Horowitz, L. W., Isaksen, I. S. A., Lawrence, M. G., Montanaro, V., Müller, J.-F., Pitari, G., Prather, M. J., Pyle, J. A., Rast, S., Rodriguez, J. M., Sanderson, M. G., Savage, N. H., Strahan, S. E., Sudo, K., Szopa, S., Unger, N., van Noije, T. P. C., and Zeng, G.: Multimodel simulations of carbon monoxide: Comparison with observations and projected near-future changes, Journal of Geophysical Research: Atmospheres, 111, n/a–n/a, doi:10.1029/2006JD007100, http://dx.doi.org/10.1029/2006JD007100, 2006.

Singh, H. B. and Hanst, P. L.: Peroxyacetyl nitrate (PAN) in the unpolluted atmosphere: An important reservoir for nitrogen oxides, Geophysical Research Letters, 8, 941–944, doi:10.1029/GL008i008p00941, http://dx.doi.org/10.1029/GL008i008p00941, 1981.

Spada, M., Jorba, O., Pérez García-Pando, C., Janjic, Z., and Baldasano, J. M.: Modeling and evaluation of the global sea-salt aerosol distribution: sensitivity to size-resolved and sea-surface temperature dependent emission schemes, Atmospheric Chemistry and Physics, 13, 11 735–11 755, doi:10.5194/acp-13-11735-2013, http://www.atmos-chem-phys.net/13/11735/2013/, 2013.

Geoscientific
Model Development
Discussions

Spada, M., Jorba, O., García-Pando, C. P., Janjic, Z., and Baldasano, J.: On the evaluation of global sea-salt aerosol models at coastal/orographic sites, Atmospheric Environment, 101, 41 – 48, doi:http://dx.doi.org/10.1016/j.atmosenv.2014.11.019, http://www.sciencedirect.com/science/article/pii/S1352231014008784, 2015.

Spada, M., Jorba, O., Pérez García-Pando, C., Tsigaridis, K., Soares, J., and Janjic, Z.: Global aerosols in the online multiscale NMMB/BSC Chemical Transport Model, in prep.

Spivakovsky, C. M., Logan, J. A., Montzka, S. A., Balkanski, Y. J., Foreman-Fowler, M., Jones, D. B. A., Horowitz, L. W., Fusco, A. C., Brenninkmeijer, C. A. M., Prather, M. J., Wofsy, S. C., and McElroy, M. B.: Three-dimensional climatological distribution of tropospheric OH: Update and evaluation, Journal of Geophysical Research: Atmospheres, 105, 8931–8980, doi:10.1029/1999JD901006, http://dx.doi.org/10.1029/1999JD901006, 2000.

Stein, O., Schultz, M. G., Bouarar, I., Clark, H., Huijnen, V., Gaudel, A., George, M., and Clerbaux, C.: On the wintertime low bias of Northern Hemisphere carbon monoxide found in global model simulations, Atmospheric Chemistry and Physics, 14, 9295–9316, doi:10.5194/acp-14-9295-2014, http://www.atmos-chem-phys.net/14/9295/2014/, 2014.

Stevenson, D. S., Dentener, F. J., Schultz, M. G., Ellingsen, K., van Noije, T. P. C., Wild, O., Zeng, G., Amann, M., Atherton, C. S., Bell, N., Bergmann, D. J., Bey, I., Butler, T., Cofala, J., Collins, W. J., Derwent, R. G., Doherty, R. M., Drevet, J., Eskes, H. J., Fiore, A. M., Gauss, M., Hauglustaine, D. A., Horowitz, L. W., Isaksen, I. S. A., Krol, M. C., Lamarque, J.-F., Lawrence, M. G., Montanaro, V., Müller, J.-F., Pitari, G., Prather, M. J., Pyle, J. A., Rast, S., Rodriguez, J. M., Sanderson, M. G., Savage, N. H., Shindell, D. T., Strahan, S. E., Sudo, K., and Szopa, S.: Multimodel ensemble simulations of present-day and near-future tropospheric ozone, Journal of Geophysical Research: Atmospheres, 111, n/a–n/a, doi:10.1029/2005JD006338, http://dx.doi.org/10.1029/2005JD006338, 2006.

Stohl, A., Bonasoni, P., Cristofanelli, P., Collins, W., Feichter, J., Frank, A., Forster, C., Gerasopoulos, E., Gäggeler, H., James, P., Kentarchos, T., Kromp-Kolb, H., Krüger, B., Land, C., Meloen, J., Papayannis, A., Priller, A., Seibert, P., Sprenger, M., Roelofs, G. J., Scheel, H. E., Schnabel, C., Siegmund, P., Tobler, L., Trickl, T., Wernli, H., Wirth, V., Zanis, P., and Zerefos, C.: Stratosphere-troposphere exchange: A review, and what we have learned from STACCATO, Journal of Geophysical Research: Atmospheres, 108, n/a–n/a, doi:10.1029/2002JD002490, http://dx.doi.org/10.1029/2002JD002490, 2003.

Tang, Y., M. J., Lu, S., Black, T. and, J. Z., Iredell, M., Perez, C., and O., J.: Recent status of NEMS/NMMB-AQ development, paper presented at 8th Annual CMAS Conference, U.S. Environ. Prot. Agency, Chapel Hill, N. C., 2009.

Thompson, A. M., Witte, J. C., McPeters, R. D., Oltmans, S. J., Schmidlin, F. J., Logan, J. A., Fujiwara, M., Kirchhoff, V. W. J. H., Posny, F., Coetzee, G. J. R., Hoegger, B., Kawakami, S., Ogawa, T., Johnson, B. J., Vömel, H., and Labow, G.: Southern Hemisphere Additional Ozonesondes (SHADOZ) 1998–2000 tropical ozone climatology 1. Comparison with Total Ozone Mapping Spectrometer (TOMS) and ground-based measurements, Journal of Geophysical Research: Atmospheres, 108, doi:10.1029/2001JD000967, http://dx.doi.org/10.1029/2001JD000967, 2003a.

Thompson, A. M., Witte, J. C., Oltmans, S. J., Schmidlin, F. J., Logan, J. A., Fujiwara, M., Kirchhoff, V. W. J. H., Posny, F., Coetzee, G. J. R., Hoegger, B., Kawakami, S., Ogawa, T., Fortuin, J. P. F., and Kelder, H. M.: Southern Hemisphere Additional Ozonesondes (SHADOZ) 1998–2000 tropical ozone climatology 2. Tropospheric variability and the zonal wave-one, Journal of Geophysical Research: Atmospheres, 108, n/a–n/a, doi:10.1029/2002JD002241, http://dx.doi.org/10.1029/2002JD002241, 2003b.

Tilmes, S., Lamarque, J.-F., Emmons, L. K., Conley, A., Schultz, M. G., Saunois, M., Thouret, V., Thompson, A. M., Oltmans, S. J., Johnson, B., and Tarasick, D.: Technical Note: Ozonesonde climatology between 1995 and 2011: description, evaluation and applications, Atmospheric Chemistry and Physics, 12, 7475–7497, doi:10.5194/acp-12-7475-2012, http://www.atmos-chem-phys.net/12/7475/2012/, 2012.

Turquety, S., Clerbaux, C., Law, K., Coheur, P.-F., Cozic, A., Szopa, S., Hauglustaine, D. A., Hadji-Lazaro, J., Gloudemans, A. M. S., Schrijver, H., Boone, C. D., Bernath, P. F., and Edwards, D. P.: CO emission and export from Asia: an analysis combining complementary satellite measurements (MOPITT, SCIAMACHY and ACE-FTS) with global modeling, Atmospheric Chemistry and Physics, 8, 5187–5204, doi:10.5194/acp-8-5187-2008, http://www.atmos-chem-phys.net/8/5187/2008/, 2008.

5 Val Martin, M., Heald, C. L., and Arnold, S. R.: Coupling dry deposition to vegetation phenology in the Community Earth System Model: Implications for the simulation of surface O_3, Geophysical Research Letters, 41, 2988–2996, doi:10.1002/2014GL059651, http://dx.doi.org/10.1002/2014GL059651, 2014.

Van Aardenne, J. A., Dentener, F. J., Olivier, J. G. J., and Peters, J. A. H. W.: The EDGAR 3.2 Fast Track 2000 dataset (32FT2000), Tech. rep., http://www.mnp.nl/edgar/model/v32ft2000edgar/docv32ft20, 2005.

10 Voulgarakis, A., Naik, V., Lamarque, J.-F., Shindell, D. T., Young, P. J., Prather, M. J., Wild, O., Field, R. D., Bergmann, D., Cameron-Smith, P., Cionni, I., Collins, W. J., Dalsøren, S. B., Doherty, R. M., Eyring, V., Faluvegi, G., Folberth, G. A., Horowitz, L. W., Josse, B., MacKenzie, I. A., Nagashima, T., Plummer, D. A., Righi, M., Rumbold, S. T., Stevenson, D. S., Strode, S. A., Sudo, K., Szopa, S., and Zeng, G.: Analysis of present day and future OH and methane lifetime in the ACCMIP simulations, Atmospheric Chemistry and Physics, 13, 2563–2587, doi:10.5194/acp-13-2563-2013, http://www.atmos-chem-phys.net/13/2563/2013/, 2013.

15 Vukovic, A., R. B. and Z., J.: Land ice sea surface model: Short description and verification, , paper presented at 2010 International Congress on Environmental Modelling and Software Modelling for Environment's Sake, Int. Environ. Modell. and Software Soc., Ottaw, 2010.

Wesely, M.: Parameterization of surface resistances to gaseous dry deposition in regional-scale numerical models , Atmospheric Environment (1967), 23, 1293 – 1304, doi:http://dx.doi.org/10.1016/0004-6981(89)90153-4, http://www.sciencedirect.com/science/article/pii/0004698189901534, 1989.

20 Wesely, M. and Hicks, B.: A review of the current status of knowledge on dry deposition, Atmospheric Environment, 34, 2261 – 2282, doi:http://dx.doi.org/10.1016/S1352-2310(99)00467-7, http://www.sciencedirect.com/science/article/pii/S1352231099004677, 2000.

WHO: Ambient (outdoor) air quality and health, http://www.who.int/mediacentre/factsheets/fs313/en/, 2014.

Wild, O., Zhu, X., and Prather, M. J.: Fast-J: Accurate Simulation of In- and Below-Cloud Photolysis in Tropospheric Chemical Models, Journal of Atmospheric Chemistry, 37, 245–282, doi:10.1023/A:1006415919030, http://dx.doi.org/10.1023/A%3A1006415919030, 2000.

25 Wotawa, G., Novelli, P. C., Trainer, M., and Granier, C.: Inter-annual variability of summertime CO concentrations in the Northern Hemisphere explained by boreal forest fires in North America and Russia, Geophysical Research Letters, 28, 4575–4578, doi:10.1029/2001GL013686, http://dx.doi.org/10.1029/2001GL013686, 2001.

Yarwood, G., Rao, S., Yocke, M., and Whitten, G.: Updates to the Carbon Bond Chemical Mechanism: CB05. Final Report to the US EPA, RT-0400675, http://www.camx.com/publ/pdfs/CB05_Final_Report_120805.pdf, 2005.

30 Young, P. J., Archibald, A. T., Bowman, K. W., Lamarque, J.-F., Naik, V., Stevenson, D. S., Tilmes, S., Voulgarakis, A., Wild, O., Bergmann, D., Cameron-Smith, P., Cionni, I., Collins, W. J., Dalsøren, S. B., Doherty, R. M., Eyring, V., Faluvegi, G., Horowitz, L. W., Josse, B., Lee, Y. H., MacKenzie, I. A., Nagashima, T., Plummer, D. A., Righi, M., Rumbold, S. T., Skeie, R. B., Shindell, D. T., Strode, S. A., Sudo, K., Szopa, S., and Zeng, G.: Pre-industrial to end 21st century projections of tropospheric ozone from the Atmospheric Chemistry and Climate Model Intercomparison Project (ACCMIP), Atmospheric Chemistry and Physics, 13, 2063–2090, doi:10.5194/acp-13-2063-2013,
35 http://www.atmos-chem-phys.net/13/2063/2013/, 2013.

Zhang, Y.: Online-coupled meteorology and chemistry models: history, current status, and outlook, Atmospheric Chemistry and Physics, 8, 2895–2932, doi:10.5194/acp-8-2895-2008, http://www.atmos-chem-phys.net/8/2895/2008/, 2008.

Zilitinkevich, S.: Bulk characteristics of turbulence in the atmospheric planetary boundary layer, Tr. GGO, 167, 49–52, 1965.

Geoscientific
Model Development
Discussions
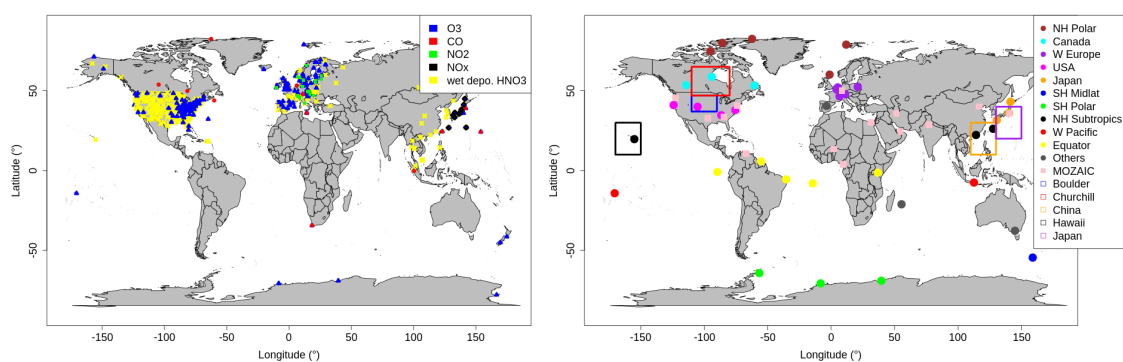
Figure 1. Stations used for the evaluation of the NMMB/BSC-CTM model. On the left, surface-monitoring rural stations of O_3 (blue triangle), CO (red circle), NO_2 (green square cross) and NO_X (black diamond) are shown. Moreover, wet deposition HNO_3 (yellow cross) measurement locations are presented. On the right, locations of the different ozonesondes used (O_3 vertical profiles) are shown. Ozonesonde are grouped by the following regions: NH Polar (brown circle), Canada (cyan circle), W. Europe (purple circle), USA (pink circle), Japan (orange circle), SH Midlat (blue circle), SH Polar (green circle), NH Subtropics (black circle), W. Pacific (red circle), Equator (yellow circle) and Others (grey circle). In addition, CO vertical profiles from the aircraft campaign MOZAIC (pink square) are presented. Finally, large rectangles show areas for the climatology analysis (NO_x, PAN and HNO_3) of Boulder (blue), Churchill (red), China (orange), Hawaii (black) and Japan (purple).
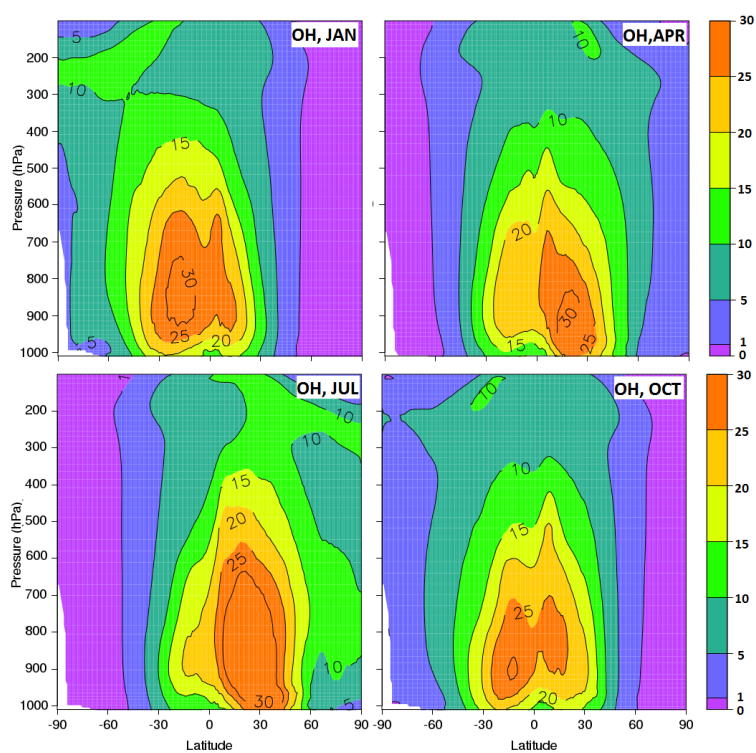
Figure 2. Zonally monthly mean OH concentrations (10^5 molecules / cm^{-3}) for January, April, July and October by the NMMB/BSC-CTM model

Geoscientific
Model Development
Discussions
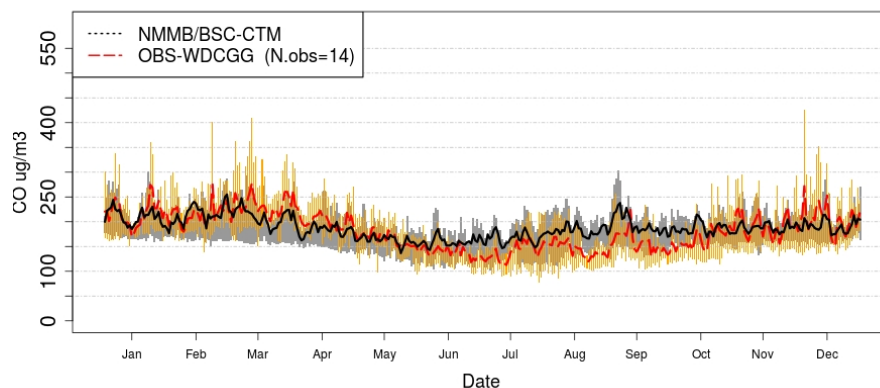
Figure 3. Time series of CO daily mean concentration in $\mu g\ m^{-3}$, averaged over all the rural WDCGG stations used. Observations are in a solid red line and model data in a solid black line. Bars show the 25th-75th quartile interval for observations (orange bars) and for model simulation (grey bars).
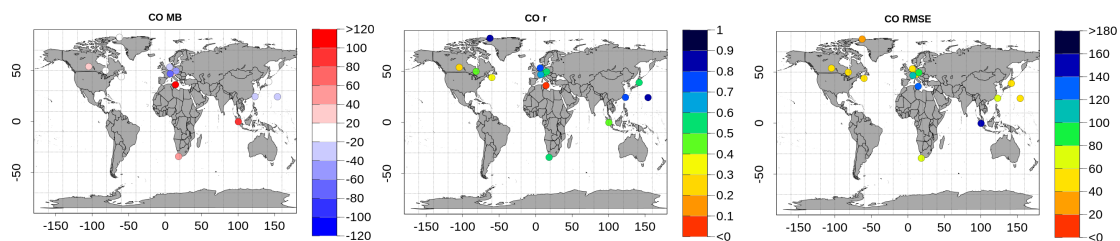

Figure 4. CO spatial distribution of mean bias (MB, %) (left panel) , correlation (r) (middle panel) and root mean square error (RMSE,μg m^{-3}) (right panel) at all rural WDCGG stations used.

Geoscientific
Model Development
Discussions
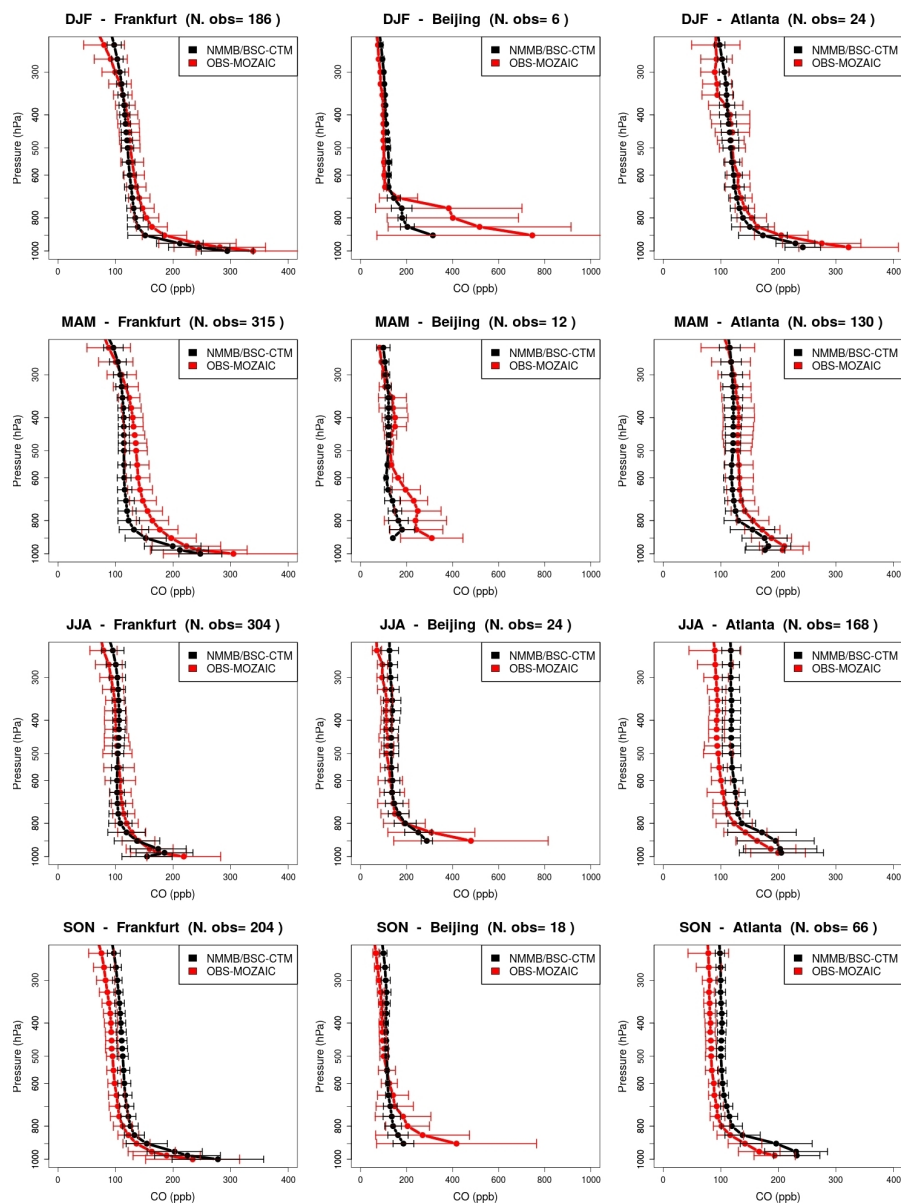
Figure 5. CO vertical profile seasonal averages over Frankfurt, Beijing and Atlanta (from left to right) for the whole year 2004. Observations are in a solid red line and model data in a solid black line. The number of observations flights is given on the top of each plot.
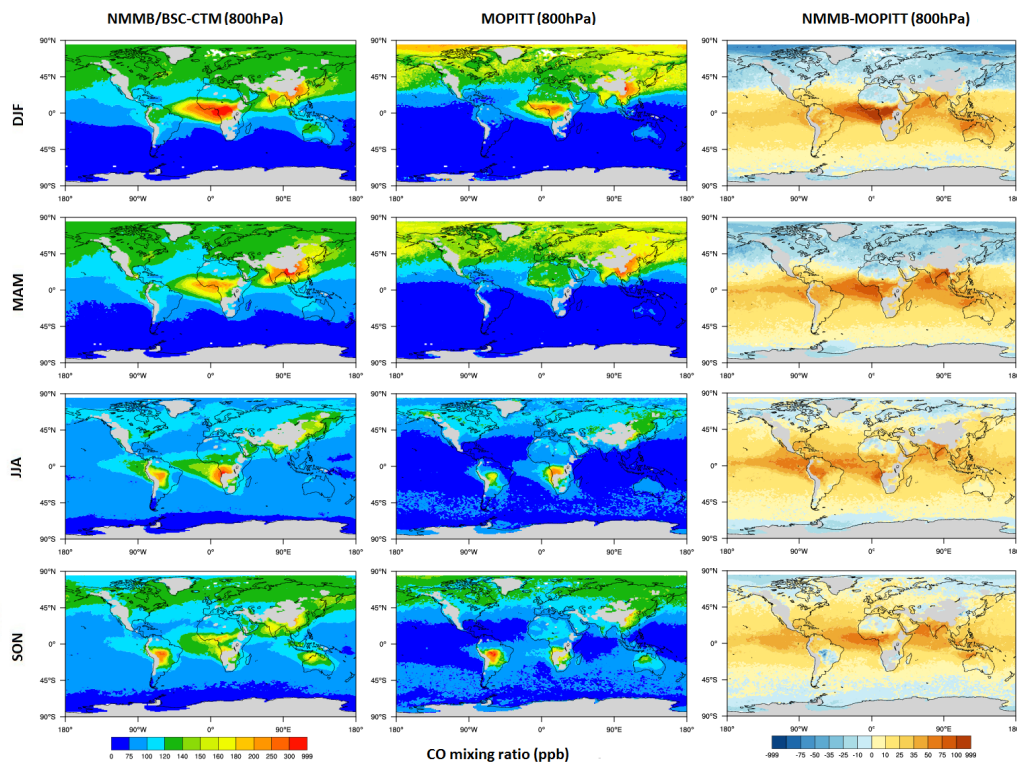
Figure 6. Comparison of modelled NMMB/BSC-CTM CO mixing ratio at 800 hPa against satellite data (MOPITT) for (from top) (DJF for December-January-February, MAM for March-April-May, JJA for June-July-August and SON for September-October-November) for the whole year 2004 in ppb. NMMB/BSC-CTM data is displayed in the left panel, MOPITT data in the middle panel and the bias in the right panel.

Geoscientific
Model Development
Discussions
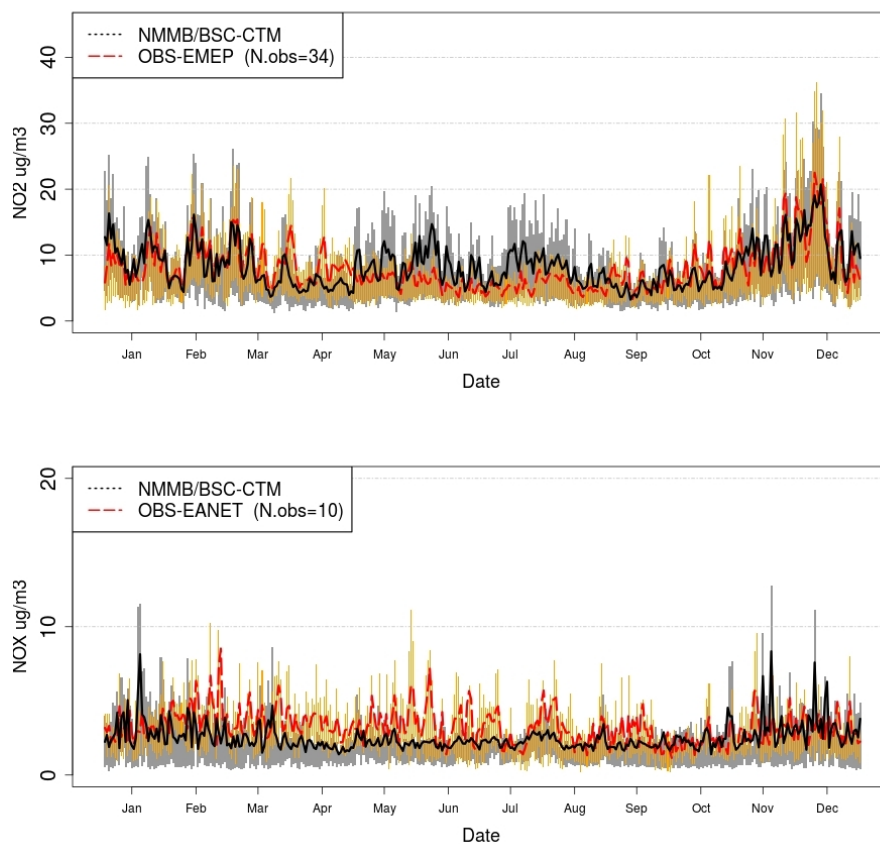
Figure 7. Time series of NO$_2$ (top) and NO$_x$ (bottom) daily mean concentration averaged over all the rural EMEP and EANET stations, respectively, used in μg m^{-3}. Observations are in a solid red line and model data in a solid black line. Bars show the 25th-75th quartile interval for observations (orange bars) and for model simulation (grey bars).
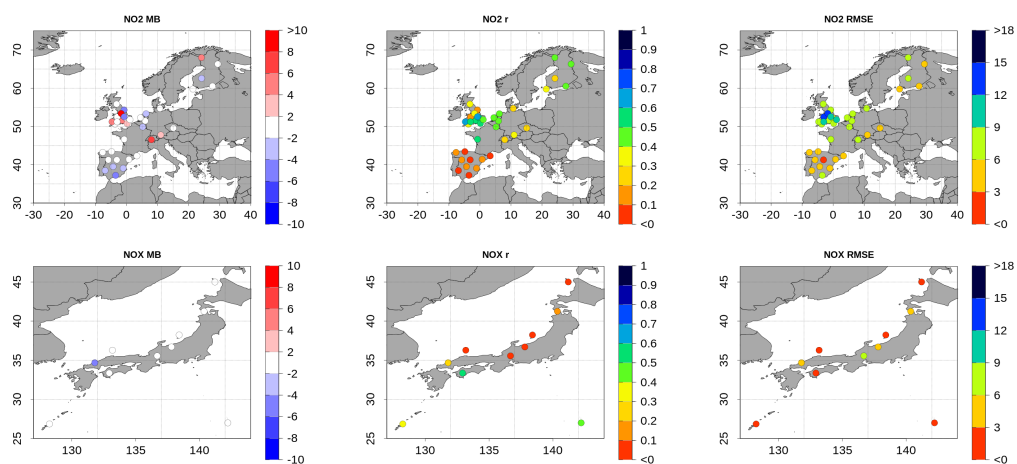
Figure 8. NO$_2$ (top) NO$_x$ (bottom) and spatial distribution of mean bias (MB, %) (left panel) , correlation (r) (middle panel) and root mean square error (RMSE, μg m^{-3}) (right panel) at all rural EMEP and EANET, respectively, stations used

Geoscientific
Model Development
Discussions

Open Access

EGU
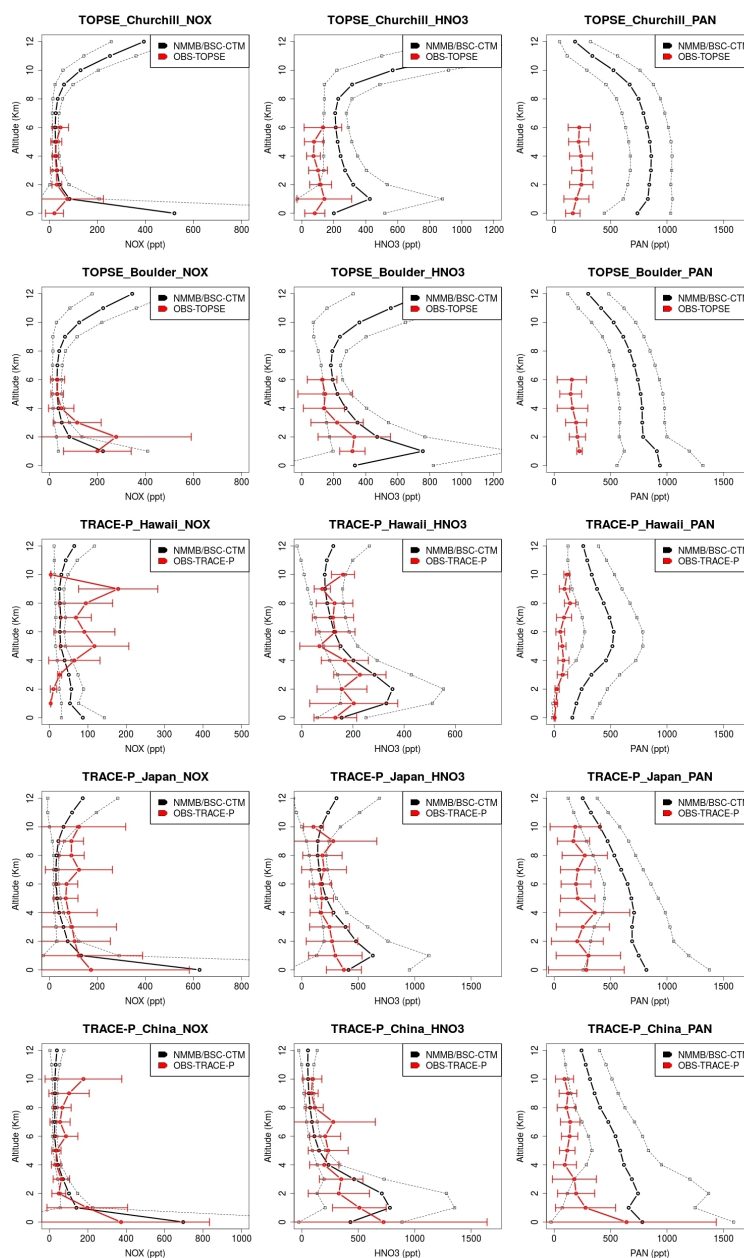
Figure 9. Comparison of modeled (black lines) and observed (red lines) vertical profiles of NO_X (first column), HNO_3 (second column) and PAN (third column) for several regions over US, China, Hawaii and Japan.
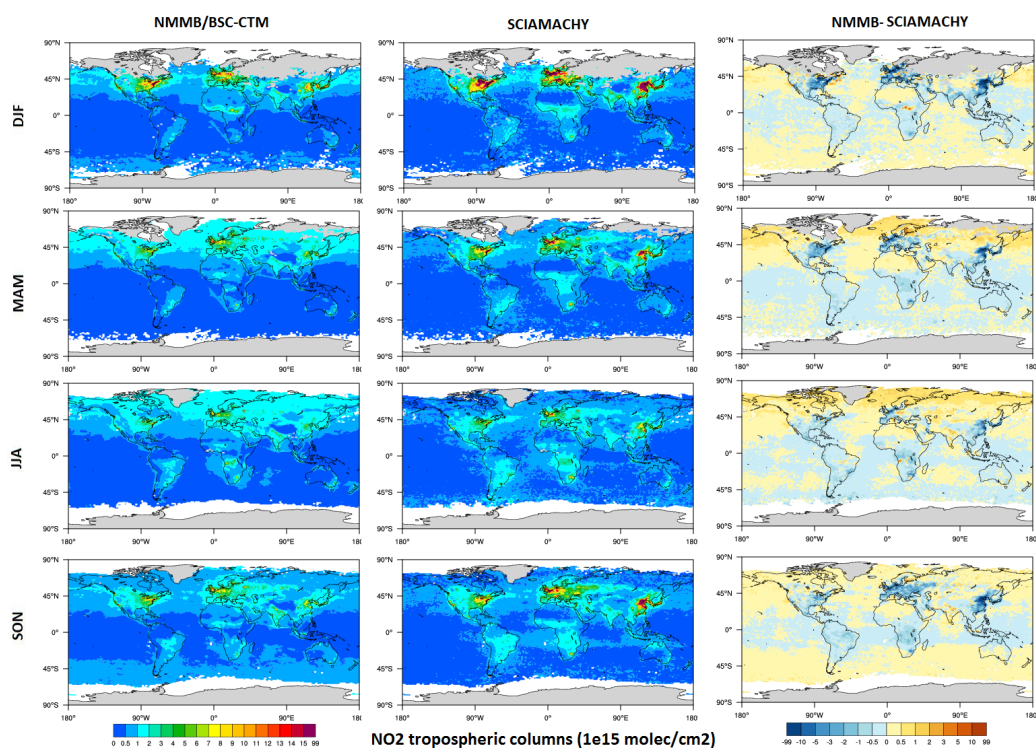
Figure 10. Comparison of modelled NMMB/BSC-CTM NO_2 vertical tropospheric columns against satellite data (SCIAMACHY) for (from top) DJF, MAM, JJA, and SON for the entire year 2004 in $1e^{15}$ molec/cm^2 . NMMB/BSC-CTM data is displayed in the left panel, SCIA-MACHY data in the middle panel and the bias in the right panel.
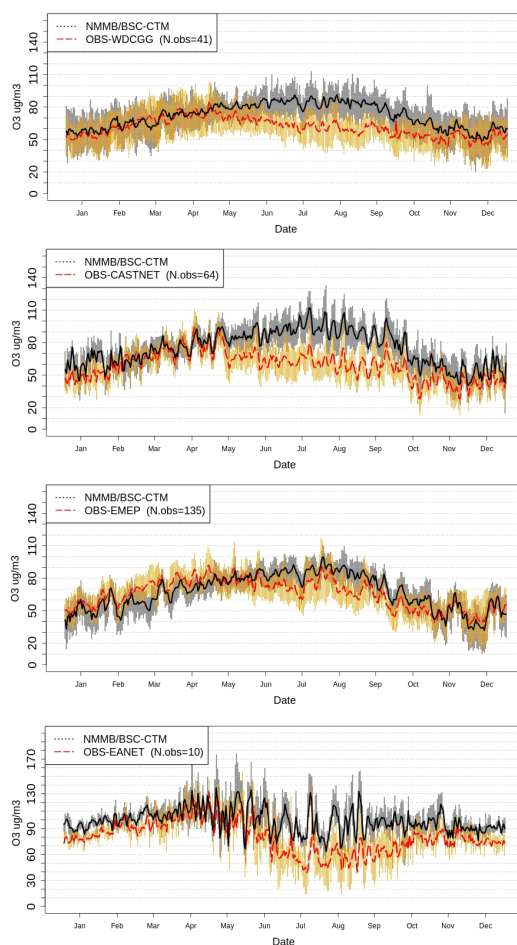
Figure 11. Time series of O$_3$ daily mean concentration averaged over all the rural WDCGG, CASTNET, EMEP and EANET stations (from top to bottom) used in μg m^{-3}. Observations are in a solid red line and model data in a solid black line. Bars show the 25th-75th quartile interval for observations (orange bars) and for model simulation (grey bars).
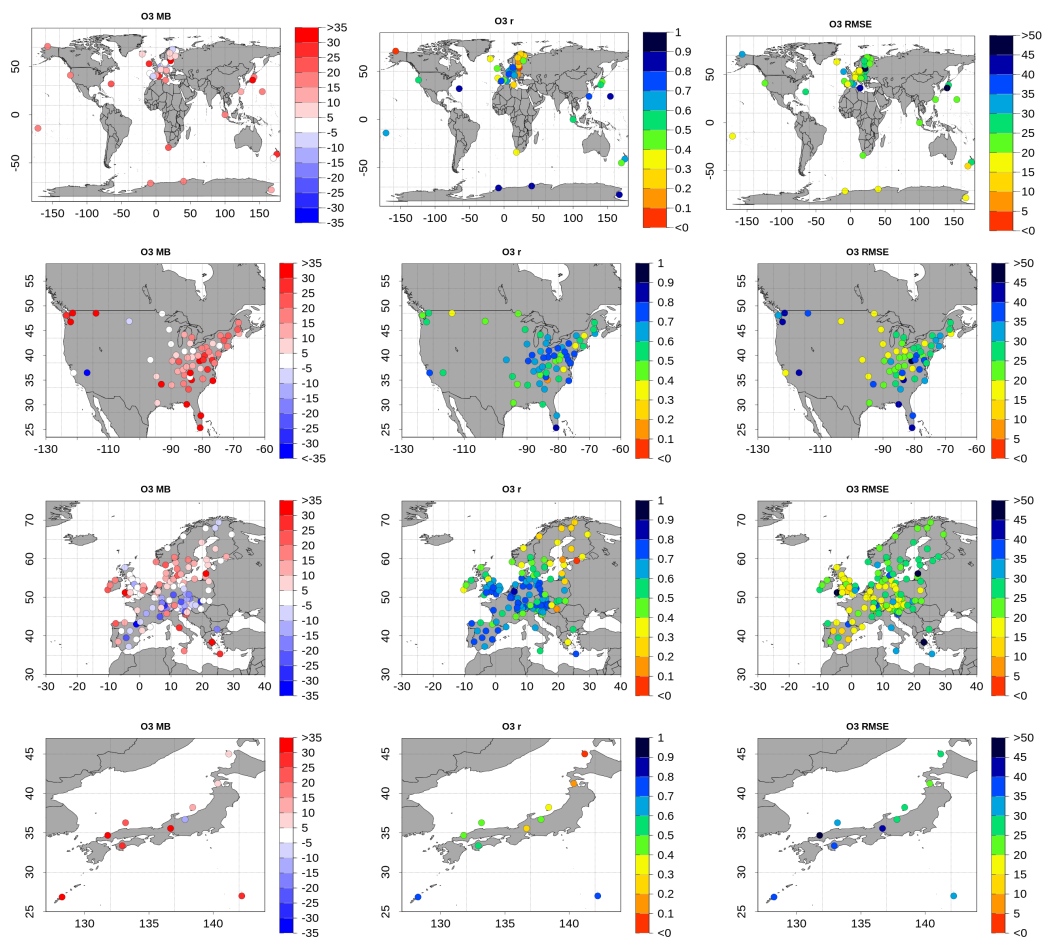
Figure 12. O$_3$ spatial distribution of mean bias (MB, %) (left panel) , correlation (r) (middle panel) and root mean square error (RMSE, μg m^{-3}) (right panel) at all rural WDCGG, CASTNET, EMEP and EANET (from top to bottom) stations used.
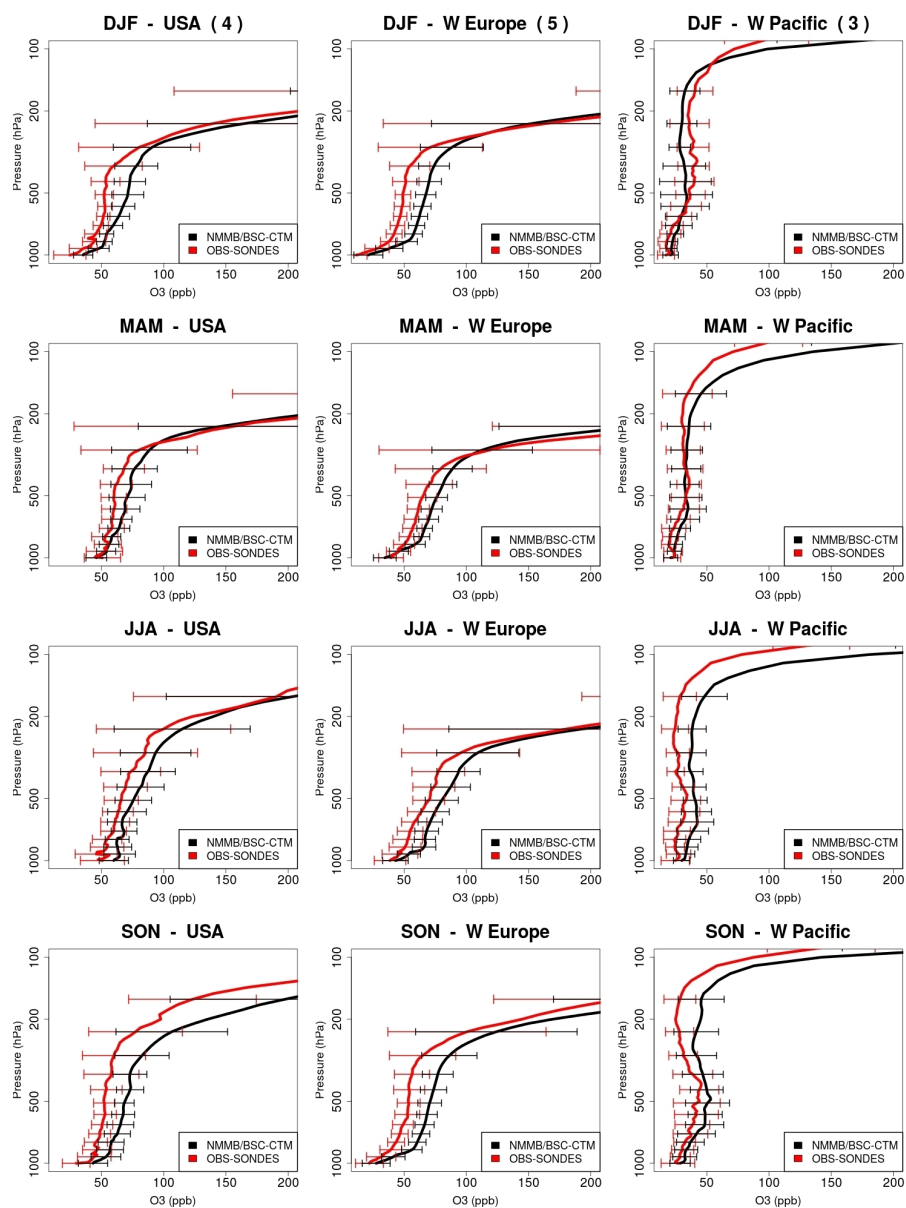
**Figure 13.** Comparison of ozonesonde measurements (red lines) and simulated (black lines) seasonal vertical profiles of O$_3$ (ppb) and standard deviations (horizontal lines). The region name and the number of stations, using brackets, are given above each plot.
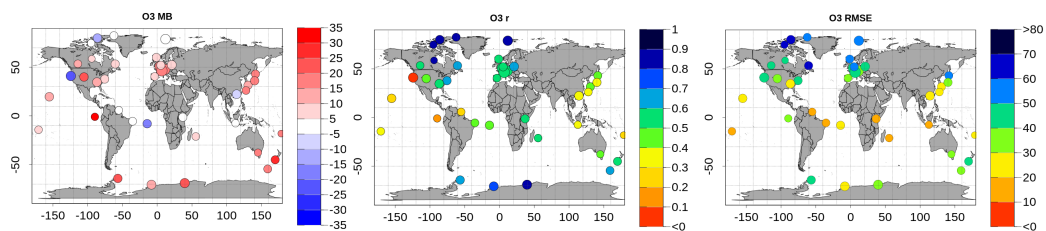
Figure 14. Mean tropospheric ozone bias spatial distribution of NMMB/BSC-CTM minus ozonesondes (MB, %) (left panel), root mean square error (RMSE, μg m^{-3}) (middle panel) and correlation (right panel) for the whole 2004, averaged between 400-1000 hPa. The diameter of the circles indicates the number of profiles over the respective stations.

Table 1. Model characteristics and experiment configuration

Meteorology	
Dynamics	non-hydrostatic NMMB (Janjic and Gall, 2012)
Physics	Ferrier microphysics (Ferrier et al., 2002)
	BMJ cumulus scheme (Betts and Miller, 1986)
	MYJ PBL scheme (Janjic et al., 2001)
	LISS land surface model (Vukovic and Z., 2010)
	RRTMG radiation (Mlawer et al., 1997)
Chemistry	
Chemical mechanism	Carbond Bond 05 (Yarwood et al., 2005)
Photolysis scheme	online Fast-J photolysis scheme (Wild et al., 2000)
Aerosols	No aerosols considered in this study
Dry deposition	Wesley resistance approach from Wesely (1989)
Wet deposition	Grid and sub-grid scale from Foley et al. (2010)
Biogenic emissions	MEGAN (Guenther et al., 2006)
Anthropogenic and other natural emissions	ACCMIP (Lamarque et al., 2010) and POET (Granier et al., 2005)
Stratospheric ozone	COPCAT (Monge-Sanz et al., 2011)
Resolution and Initial conditions	
Horizontal resolution	1.4° x 1°
Vertical layers	64
Top of the atmosphere	1 hPa
Chemical initial condition	MOZART4 (Emmons et al., 2010)
Meteorological initial condition	FNL/NCEP
Chemistry spin-up	1 year

Table 2. Emissions totals by category for 2004 in Tg(species)/year. Anthropogenic and biomass burning applied in this study are based on Lamarque et al. (2013). Ocean and soil natural emissions are based on the POET (Granier et al., 2005) global inventory. Biogenic emissions are computed online from the MEGAN (Guenther et al., 2006).

Species	Anthrop.	Bio. burning	Biogenic	Soil	Ocean
CO	610.5	459.6	148.13	-	19.85
NO	85.8	5.4	16.54	11.7	-
SO_2	92.96	3.84	-	-	-
Isoprene (C_5H_8)	-	0.15	683.16	-	-
Terpene ($C_{10}H_6$)	-	0.03	120.85	-	-
Xylenes (C_8H_{10})	1.05	0.16	1.36	-	-
Methanol (CH_3OH)	-	-	159.91	-	-
Ethanol (C_2H_6O)	4.28	3.7	17.06	-	-
Formaldehyde (HCHO)	4.24	0.35	9.58	-	-
Aldehyde (R-CHO)	-	-	5.06	-	-
Toluene (C_7H_8)	0.66	0.19	0.79	-	-
Ethane (C_2H_6)	1.27	0.57	0.48	-	-
Ethylene (C_2H_4)	3.32	2.71	32.03	-	-

Table 3. Ozonesondes main information used in this model evaluation for the year 2004. Location of these ozonesondes is displayed in the third and fourth columns. Columns 6-9 display the number of available measurements for each season (DJF for December-January-February, MAM for March-April-May, JJA for June-July-August and SON for September-October-November).

Station	Country	Latitude	Longitude	Region	DJF	MAM	JJA	SON
Kagoshima	Japan	31.6N	130.6E	Japan	13	12	11	12
Saporo	Japan	43.1N	141.3E	Japan	12	10	12	10
Tsukubay	Japan	36.1N	140.1E	Japan	14	13	12	12
Alert	Canada	82.5N	62.3W	NH Polar	11	10	13	9
Edmonton	Canada	53.5N	114.1W	Canada	7	12	10	10
Resolute	Canada	74.8N	95.0W	NH Polar	9	10	8	6
Macquarie Island	Australia	54.5S	158.9E	SH Midlat	6	15	12	9
Lerwick	Great Britain	60.1N	1.2W	W Europe	9	13	13	12
Uccle	Belgium	50.8N	4.3E	W Europe	35	37	36	36
Goose Bay	Canada	53.3N	60.4W	Canada	12	13	13	12
Churchill	Canada	58.7N	94.1W	Canada	7	6	4	8
NyAlesund	Norway	78.9N	11.9E	NH Polar	25	24	23	17
Hohenpeissenberg	Deutschland	47.8N	11.0E	Europe	34	34	26	31
Syowa	Japan (Antarctica)	69.0S	39.6E	SH Polar	16	16	19	26
Wallops Island	USA	37.9N	75.5W	USA	11	15	17	7
Hilo	USA	19.7N	155.1W	NH Subtropic	13	18	14	12
Payerne	Switzerland	46.5N	6.6E	Europe	38	40	38	40
Nairobi	Kenya	1.3S	36.8E	Equador	11	13	13	13
Naha	Japan	26.17N	127.7E	NH Subtropics	9	12	8	10
Samoa	Independent State of Samoa	14.2S	170.6W	W Pacific	9	11	8	9
Legionowo	Poland	52.4N	20.9E	Europe	16	18	16	18
Marambio	Antarctica	64.2S	56.6W	SH Polar	10	7	15	22
Lauder	New Zealand	45.0S	169.7E	SH Midlat	11	13	13	9
Madrid	Spain	40.5N	3.6W	Others	11	9	8	12
Eureka	Canada	80.0N	85.9W	NH Polar	17	17	11	13
De Bilt	Nederland	52.1N	5.2E	Europe	13	10	14	12
Neumayer	Antarctica	70.7S	8.3W	SH Polar	11	13	13	31
Hong Kong	China	22.3N	114.2E	NH Subtropics	12	26	11	13
Broad Meadows	Australia	37.7S	144.9E	Others	6	7	7	11
Huntsville	USA	34.7N	86.6W	USA	14	13	23	13
Parambio	Surinam	5.8N	55.2W	Equador	11	8	9	9
Reunion Island	France	21.1S	55.5E	Others	9	14	9	6
Watukosek	Indonesia	7.5S	112.6E	W Pacific	7	11	10	6
Natal	Brasil	5.5S	35.41W	Equador	10	12	13	7
Ascencion Island	Great Britain	7.98S	14.42W	Equador	12	12	12	18
San Cristobal	Galapagos	0.92S	89.6W	Equador	7	4	10	13
Boulder	USA	40.0N	105.26W	USA	12	11	17	16
Trinidad Head	USA	40.8N	124.2W	USA	4	7	5	8
Suva	Fiji	18.13S	178.4E	W Pacific	13	12	48	11

Table 4. MOZAIC aircraft information used in this model evaluation for the year 2004. Location of the MOZAIC measurements is displayed in the third and fourth columns. Columns 5-8 display the number of available measurements for each season (DJF for December-January-February, MAM for March-April-May, JJA for June-July-August and SON for September-October-November).

Station	Country	Latitude	Longitude	DJF	MAM	JJA	SON
Abu Dhabi	United Arab Emirates	24.44N	54.65E	11	17	58	20
Atlanta	USA	33.63N	84.44W	24	130	168	66
Beijing	China	40.09N	116.6E	5	12	23	17
Cairo	Egypt	30.11N	31.41E	19	16	2	8
Caracas	Venezuela	10.6N	67W	21	9	9	21
Dallas	USA	32.9N	97.03W	8	24	24	10
Douala	Cameroon	4.01N	9.72E	7	0	10	6
Frankfurt	Germany	50.02N	8.53E	169	295	286	192
New Delhi	India	28.56N	77.1E	30	24	72	38
New York	USA	40.7N	74.16W	79	23	41	16
Niamey	Niger	13.48N	2.18E	4	0	12	12
Portland	USA	45.59N	122.6W	5	8	5	4
Tehran	Iran	35.69N	51.32E	8	11	31	18
Tokyo	Japan	35.76N	140.38E	38	50	56	34

Table 5. Description of additional aircraft campaign data. Location of the measurements campaigns is displayed in the third and fourth columns. The fifth column lists the date of these campaigns.

Region Name	Expedition	Latitude	Longitude	Date
Boulder	TOPSE	37-47N	110-90W	5 February to 23 May 2000
Churchill	TOPSE	47-65 N	110-80W	5 February to 23 May 2000
China	TRACE-P	10-30N	110-130E	24 February to 10 April 2001
Hawaii	TRACE-P	10-30N	170-150W	24 February to 10 April 2001
Japan	TRACE-P	20-40N	130-150E	24 February to 10 April 2001

Table 6. Annual mean burden of tropospheric CO (Tg CO) in NMMB/BSC-CTM, MOZART-2 and TM5 global models

Model	Burden						Dry depo.	Reference
	Global	NH	SH	Trop.	N. Extratrop.	S. Extratrop.		
NMMB/BSC-CTM	399	221	177	229	101	67	24	This study
MOZART-2	351	210	142	199	102	50	2	Horowitz et al. (2003)
TM5	353	-	-	188	106	59	184	Huijnen et al. (2010)
C-IFS	361	-	-	-	-	-	-	Flemming et al. (2015)

Table 7. Annual mean burden, dry deposition of tropospheric O_3 and stratospheric inflow (Tg O_3) for the NMMB/BSC-CTM, MOZART-2, TM5 and LMDz-INCA, C-IFS global models, and two different Multimodel ensembles (25 and 15 global models).

Model	Burden						Dry deposition	Stratospheric inflow	Reference
	Global	NH	SH	Trop.	N. Extra.	S. Extra.			
NMMB/BSC-CTM	348	189	158	171	101	75	1201	384	This study
MOZART-2	362	203	159	203	99	60	857	343	Horowitz et al. (2003)
TM5	312	-	-	165	84	63	829	421	Huijnen et al. (2010)
LMDz-INCA	303	178	125	-	-	-	1261	715	Folberth et al. (2006)
C-IFS	390	-	-	-	-	-	-	-	Flemming et al. (2015)
Multimodel	344 ± 39	-	-	-	-	-	1003 ± 200	552 ± 168	Stevenson et al. (2006)
Multimodel	337 ± 23	-	-	-	-	-	-	-	Young et al. (2013)